OPTICAL CONVERSION PROCESSES

D. W. Trainor and S. A. Mani
Avco Everett Research Laboratory, Inc.
2385 Revere Beach Parkway
Everett MA 02149

Semi–Annual Report for Period 15 March 1977 to 15 September 1977

Sponsored by

DEFENSE ADVANCED RESEARCH PROJECTS AGENCY
DARPA Order No. 1806

Monitored by

OFFICE OF NAVAL RESEARCH
DEPARTMENT OF THE NAVY
Arlington VA 22217

FOREWORD

Contract No.: N00014-76-C-1162

DARPA Order No.: 1806 Amendment No. 36

Program Code No.: TE20

Short Title of Work: Optical Conversion Processes

Contractor: Avco Everett Research Laboratory, Inc.
Everett, Massachusetts 02149

Principal Investigator: Daniel W. Trainor, (617) 389-3000, Ext. 467

Scientific Officer: Director, Physics Program, Physical Sciences Division
Office of Naval Research
800 North Quincy Street
Arlington, Virginia 22217

Effective Date of Contract: 15 September 1976

Contract Expiration Date: 15 November 1977

Amount of Contract: $233,696

UNCLASSIFIED

SECURITY CLASSIFICATION OF THIS PAGE (When Data Entered)

REPORT DOCUMENTATION PAGE

READ INSTRUCTIONS BEFORE COMPLETING FORM

1. REPORT NUMBER

2. GOVT ACCESSION NO.

3. RECIPIENT'S CATALOG NUMBER

4. TITLE (and Subtitle)

Optical Conversion Processes

5. TYPE OF REPORT & PERIOD COVERED

Semi-Annual Report
15 March 1977 - 15 Sept 1977

6. PERFORMING ORG. REPORT NUMBER

7. AUTHOR(s)

D. W. Trainor and S. A. Mani

8. CONTRACT OR GRANT NUMBER(s)

N00014-76-C-1162
DARPA Order - 1806

9. PERFORMING ORGANIZATION NAME AND ADDRESS

Avco Everett Research Laboratory, Inc.
2385 Revere Beach Parkway
Everett, Massachusetts 02149

10. PROGRAM ELEMENT, PROJECT, TASK AREA & WORK UNIT NUMBERS

11. CONTROLLING OFFICE NAME AND ADDRESS

Defense Advanced Research Projects Agency
DARPA Order No. 1806

12. REPORT DATE

15 Sep 77

13. NUMBER OF PAGES

65

14. MONITORING AGENCY NAME & ADDRESS (if different from Controlling Office)

Office of Naval Research
Department of the Navy
Arlington, Virginia 22217

15. SECURITY CLASS. (of this report)

Unclassified

15a. DECLASSIFICATION/DOWNGRADING SCHEDULE

16. DISTRIBUTION STATEMENT (of this Report)

Approved for public release; distribution unlimited.

65p.

17. DISTRIBUTION STATEMENT (of the abstract entered in Block 20, if different from Report)

18. SUPPLEMENTARY NOTES

19. KEY WORDS (Continue on reverse side if necessary and identify by block number)

1. Wavelength Conversion
2. Stimulated Raman
3. Parametric Down Conversion
4. Resonant Absorption

20. ABSTRACT (Continue on reverse side if necessary and identify by block number)

The overall goal of this experimental program is to identify scalable techniques that efficiently convert existing high power UV lasers to lasers operating at longer wavelengths in the visible. Two nonlinear optical conversion techniques that we have considered are: stimulated Raman and parametric conversion involving the KrF laser (248 nm).

The objective of this contract is to suggest likely acceptor atoms for each technique which will thereby allow us to evaluate some of the key technical

DD FORM 1 JAN 73 1473 EDITION OF 1 NOV 65 IS OBSOLETE

UNCLASSIFIED

SECURITY CLASSIFICATION OF THIS PAGE (When Data Entered)

Ø48450

(20)
issues involved. These include: the production of receptor candidates in the gas phase (typically refractory metals), the volumetric removal of the lower laser level in the stimulated Raman approach to prevent "bottle necking" and allow recycling of the atoms during the laser pulse, and the consideration of overall system efficiency and scalability to high power.

TABLE OF CONTENTS

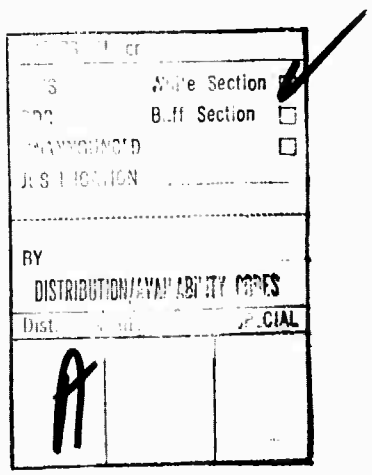

LIST OF ILLUSTRATIONS

I. INTRODUCTION

The overall goal of this combined experimental and theoretical program is to successfully and efficiently convert using scalable techniques the output of a high power KrF laser into longer wavelengths so as to vastly improve its propagation characteristics.

Since the first reported lasing of an inert gas halogen laser, a number of similar systems have demonstrated lasing characteristics. Operating at various wavelengths, with different efficiencies, a major class of electronic transition lasers came into existence. Recently, analogous mercury halide compounds showing similar formation kinetics have been shown to lase in the visible,[1,2] albeit in high temperature ($\sim 275^{\circ}C$) cells (see Figure 1). However, the most efficient laser reported to date in this group is the KrF laser operating at 248 nm. It has also produced the highest energy outputs reported utilizing e-beam pumping and e-beam controlled discharge pumping and has a demonstrated capability for being scaled to high average power. In certain applications, especially those requiring transmission through the atmosphere, its short wavelength severely limits its usefulness. This limitation in propagation at short wavelengths arises due to absorption by atmospheric ozone and to Rayleigh scattering which increases as λ^{-4} as the wavelength gets shorter. Ozone absorption is severe for wavelengths $\lesssim 3000$ Å.

---

(1) Parks, J. H., Appl. Phys. Letters 31, 192 (1977).

(2) Parks, J. H., Appl. Phys. Letters 31, 297 (1977).

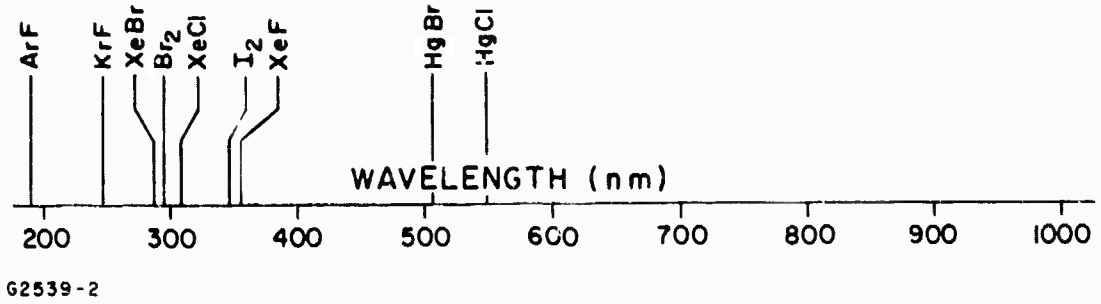

Figure 1 Demonstrated Potentially Scalable Electronic Transition Lasers

Figure 2 shows vertical transmission from a height of 3 km as a function of wavelength. Also plotted are quantum efficiency of conversion from KrF wavelengths and the total percentage transmission of converted KrF radiation. From the figure, it is apparent that to efficiently utilize KrF laser radiation, its conversion wavelength should be between 340 and 400 nm to maximize its atmospheric transmission with minimal loss from quantum yield considerations. Xenon fluoride lasers, while possessing a more attractive wavelength for propagation, have not yet demonstrated the combined efficiency and energy density comparable to KrF. Any optical conversion scheme for altering the wavelength of KrF laser radiation to the 340 to 400 nm wavelength range could have higher overall efficiency than the XeF laser if the photon conversion efficiency is $\gtrsim 40\%$. Such efficiency for conversion is a reasonable goal for the program we are discussing here. For supporting evidence, one can look over the past year at a number of milestones that have been reported relevant to the optical conversion of UV excimer lasers. With regard to overall conversion efficiency, an XeF laser has been converted, at near unit photon conversion efficiency, using barium vapor.[3] Also KrF conversion to a series of UV-visible lines due to 6 Stokes and 2 anti-Stokes transitions in high pressure molecular hydrogen was reported showing good overall conversion efficiency.[4] Also, a number of acceptor candidates identified as potential converters for KrF have been produced in the gas phase using scalable techniques.[5] In view of the above, it seems reasonable and important to pursue scalable techniques

---

(3) Djeu, N. and Burnham, R., Appl. Phys. Letters 30, 473 (1977).

(4) Loree, T.R., Sze, R.C. and Barker, D.L., Appl. Phys. Letters 31, 37 (1977).

(5) Trainor, D.W. and Mani, S.A., Optical Conversion Processes, Contract No. N00014-76-C-1162, Semi-Annual Technical Report, 15 Sept. 1976 to 15 March 1977.

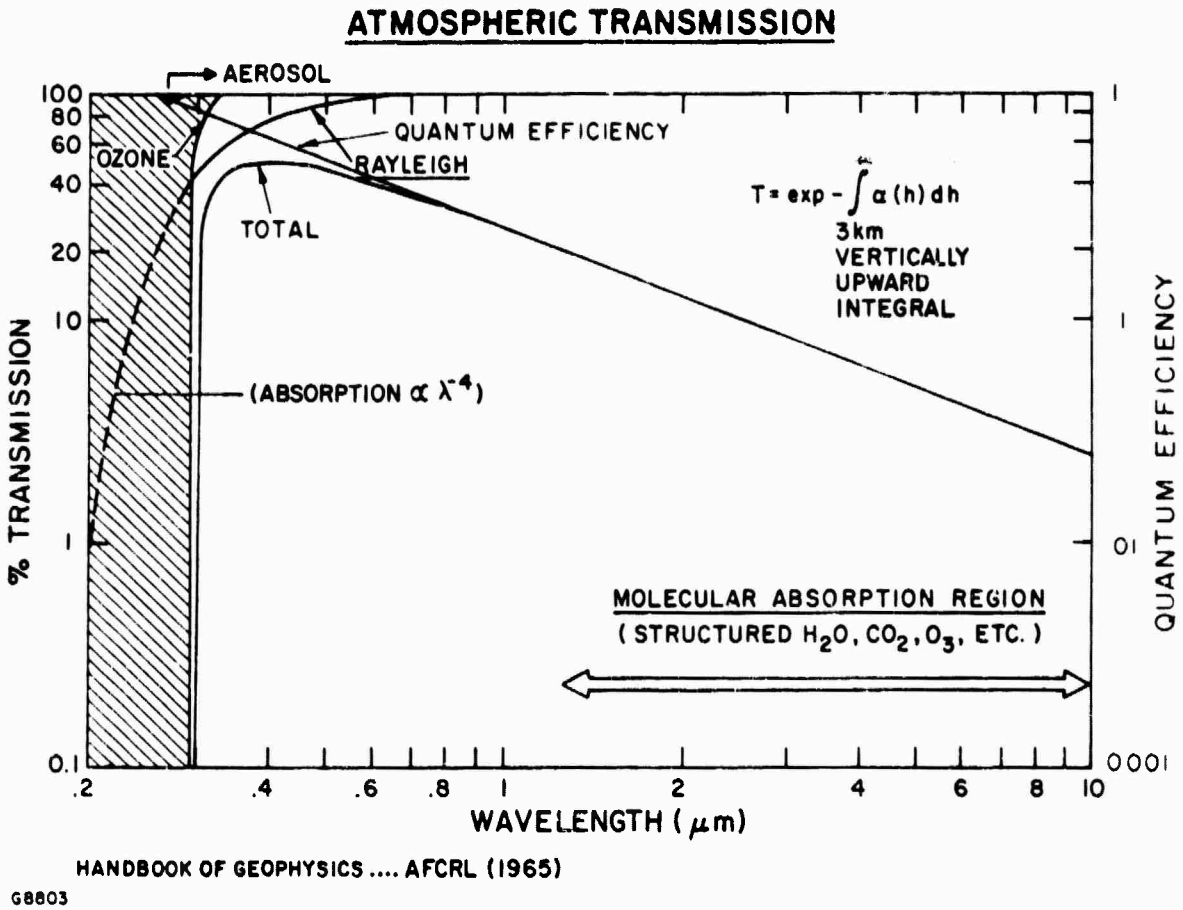

Figure 2 Propagation of Converted KrF Photons

that could efficiently convert KrF laser output to longer wavelengths. Two non-linear optical conversion techniques that we have considered to achieve this goal are stimulated Raman and parametric conversion processes.

For the stimulated Raman process, phenomenologically, the acceptor atom can be thought of as absorbing as incident KrF photon thereby making a transition to an excited virtual state and then, with the emission of a Raman photon at longer wavelengths, proceeding to a level near the ground (initial) state. Through collisions with an efficient quenching gas, it can return to the initial state for subsequent re-excitation by the KrF laser field, i.e., exhibit high efficiency by recycling the metal atoms. The Raman process is enhanced when the virtual state is close to a real state.

Another method of "down conversion" to lower energy, longer wavelength photons applicable to UV laser light is parametric down conversion. In this process, conversion is achieved by the utilization of the non-linear properties of the medium (the acceptor atom or molecules). Here an atom in state 0 upon exposure to KrF laser light of frequency ν_1 goes to a virtual state 1 and re-emits three photons of frequencies ν_2, ν_3 and ν_4 such that $\nu_1 = \nu_2 + \nu_3 + \nu_4$. At the end of this process, the atom returns to its initial state entirely by optical transitions. Once again, if the various atomic transitions (ν_1, ν_2, ν_3, and ν_4) in the acceptor are allowed and the dipole moments are large, near resonant effects enhance the overall process such that efficient down-conversion should be likely.

At AERL during the current reporting period, theoretical and experimental research have been carried out on potentially efficient scalable schemes for converting KrF photons to longer wavelengths. By theoretical calculations, we have identified a number of promising candidates to convert

the KrF laser radiation to longer wavelengths using parametric processes (see Table 1). This adds to the stimulated Raman candidates reported in Ref. 5. Experimentally, we have modified a commercial KrF laser (Tachisto Corp., Needham, MA) to provide a focused output beam of nearly a GW/cm^2 and used this laser to convert to wavelengths near 300 nm using atomic iron as the acceptor candidate.[6] The iron was produced using scalable techniques in densities sufficiently high to provide single pass amplified spontaneous emission when exposed to a field of KrF photons from an untuned laser source. In addition, we were able to demonstrate laser action in the organo-metallic precursor (i.e., the $Fe(CO)_5$). This represents a likely laser pumped photodissociation process followed by inversion of a photofragment produced in the initial step. The results of these combined theoretical and experimental efforts are summarized in the following sections of this report.

(6) Trainor, D.W. and Mani, S.A., 30th Annual Gaseous Electronics Conference, Paper #LA-3, Oct. 20, 1977.

TABLE 1. POTENTIAL CONVERSION CANDIDATES AND THEIR OUTPUT WAVELENGTHS

Candidate	Conversion Process	Output Wavelength λ, nm
Iron	Stimulated Raman	300, 304
Calcium	" "	544
Palladium	" "	332
Platinum	" "	332
Lead	" "	309
Hydrogen	" "	277, 313, 360
Thallium	Parametric Down Conversion	~380
Lead	" "	~364
Mercury	" "	~376
Lithium	" "	~680

THIS
PAGE
IS
MISSING
IN
ORIGINAL
DOCUMENT

II. THEORY

A. INTRODUCTION

The stimulated Raman process and the calculations performed for the ARPA program on optical conversion were discussed in detail in the last semi-annual report.[5] In this report, calculations performed on the four-wave parametric down conversion will be discussed. In the parametric down conversion process, an atom in state 0 interacting with the KrF laser light of frequency ν_1 goes to a virtual state 1 and remits three photons of frequencies ν_2, ν_3 and ν_4 such that $\nu_1 = \nu_2 + \nu_3 + \nu_4$ (Figure 3). At the end of this process the atom returns to the initial state entirely by optical transitions. None of the electromagnetic energy in the parametric process is absorbed by an ideal medium in contradistinction to the stimulated Raman Stokes process in which the atom is left in an excited state at the end of the nonlinear process. Thus the problem of heat removal for a large scale converter is less severe in the parametric approach.

An interesting candidate atom for the parametric down conversion of KrF laser radiation is thallium which will be used as a concrete example in the following discussion. In the down-conversion process, the photon at frequency ν_2 is initially produced by spontaneous and stimulated Raman scattering. Since there are usually several channels available for stimulated Raman scattering, one should first calculate the Raman cross section for the different possible final states of the atom and choose the one that is most probable for determining ν_2. The frequencies ν_3 and ν_4 are then chosen

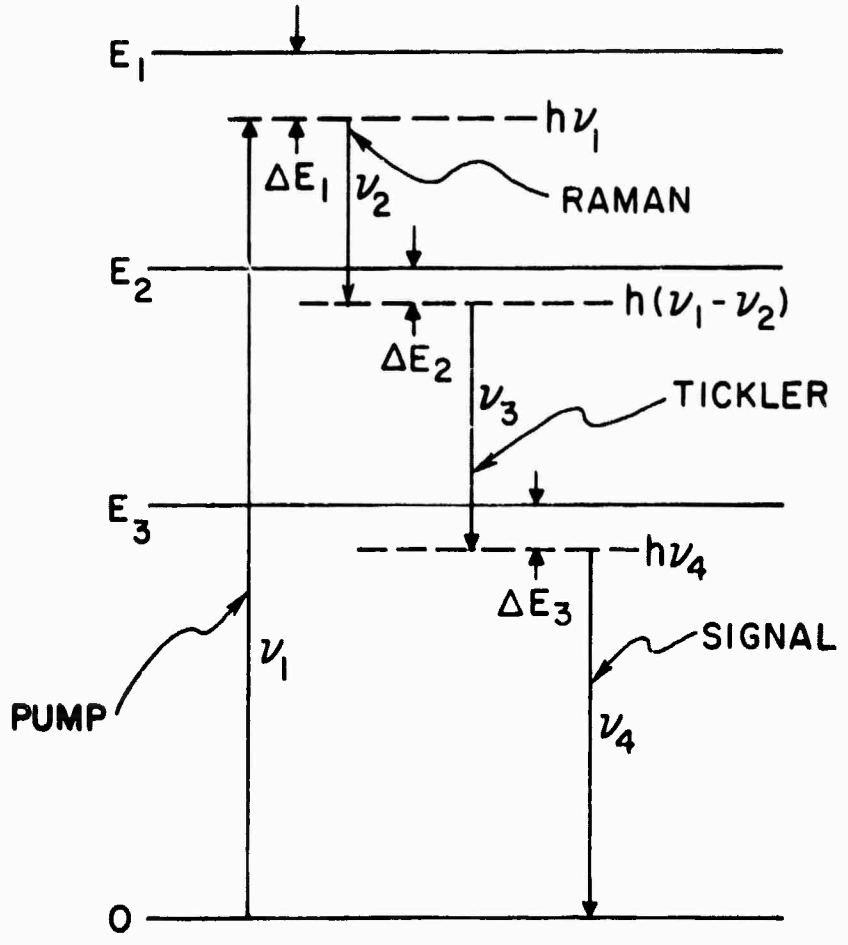

DIFFERENCE MIXING $\nu_4 = \nu_1 - \nu_2 - \nu_3$

$$\chi^{(3)} \simeq \frac{N\ \mu_{01}\ \mu_{12}\ \mu_{23}\ \mu_{30}}{(\Delta E_1)\ (\Delta E_2)\ (\Delta E_3)}$$

G2480

Figure 3 Schematic of the Parametric Down Conversion Process

to maximize the nonlinear susceptibility, $\chi^{(3)}$, subject to phase matching condition. In Section II.B, the stimulated Raman cross section is calculated for the three possible final states of a thallium atom irradiated with a KrF laser. In Section II. C, the dispersion of the four waves is calculated and phase matching is discussed. The nonlinear susceptibility, $\chi^{(3)}$, for the fourwave process is calculated in Section II. D, while in Section II. E, the coupled set of nonlinear equations for the field amplitudes is solved and the resulting conversion efficiency is calculated.

B. STIMULATED RAMAN CROSS SECTION

The energy levels of thallium atom are shown in Figure 4. Spontaneous or stimulated Raman scattering of KrF laser radiation of energy $\sim 40225\ cm^{-1}$ by an atom in the ground state can only occur to the $6p\ ^2P_{3/2}$, $7p\ ^2P_{1/2}$ or $7p\ ^2P_{3/2}$ levels. Transitions to other states are forbidden by parity selection rules. In this section, we shall calculate the stimulated Raman cross section for these three possible final states. The calculation of nonlinear susceptibilities is usually a tedious exercise. The susceptibility formulae contain products of matrix elements of the dipole operator $\vec{Q} = e\vec{r}$, of the form $< \gamma\ J\ M | \vec{Q} | \gamma'\ J'\ M' >$ which connect the initial and final atomic states through a chain of intermediate (virtual) states. Yuratich and Hanna[7] have used Racah algebra to sum over the intermediate state M values and write the nth order nonlinear susceptibility in a form that can be factorized into two parts, in one of which the relation between the fields is explicitly displayed; the other contains the physics of the atom in the form of reduced matrix elements (which can be related to oscillator strengths) and 6 j symbols In what follows, we shall use the symbols of Ref. 7 as much as possible.

(7) Yuratich, M.A. and Hanna, D. C., J. Phys. B: Atom. Molecule Phys. 9, 729 (1976).

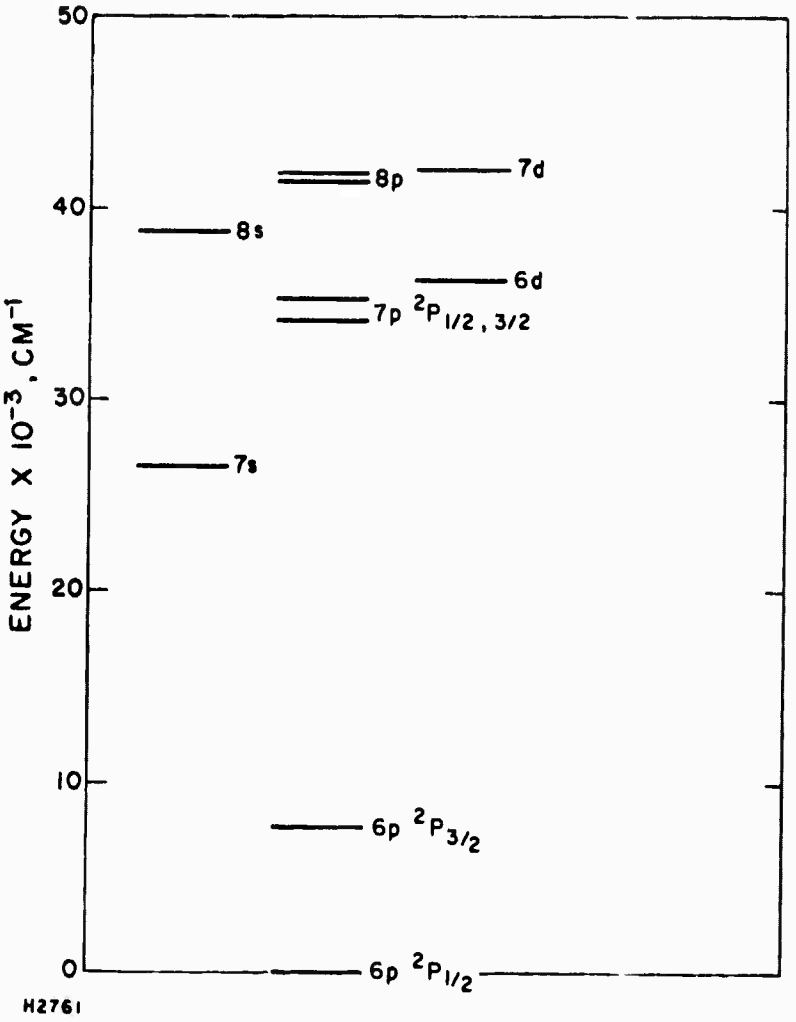

Figure 4 Energy Levels in Thallium

The Raman susceptibility χ_r per atom is given by

$$\chi_r = \frac{i}{6\,\Gamma_{ca}\,\hbar^3\,\epsilon_o}\left\{\frac{\rho_{aa}}{2J+1} - \frac{\rho_{cc}}{2J_1+1}\right\}\sum_K \Theta^{(K)}$$

$$\times \left|\sum_{\gamma_2 J_2}\begin{Bmatrix} J_1 & K & J \\ 1 & J_2 & 1 \end{Bmatrix} < \gamma_1 J_1 \|Q\| \gamma_2 J_2 > < \gamma_2 J_2 \|Q\| \gamma J >\right.$$

$$\left. \times \left[\frac{1}{\Omega_{\gamma_2 J_2 \gamma J} - \omega_p} + \frac{(-1)^K}{\Omega_{\gamma_2 J_2 \gamma J} + \omega_s}\right]\right|^2 \qquad (1)$$

In the above, ρ_{aa} and ρ_{cc} represent the initial and final state fractional populations, $2J + 1$ and $2J_1 + 1$ their corresponding degeneracies whereas $\gamma_2 J_2$ represents the intermediate states; $\Omega_{\gamma_2 J_2 \gamma J} = (E_{\gamma_2 J_2} - E_{\gamma J})/\hbar$, ω_p and ω_s are the pump and Raman frequencies respectively; $< \gamma J \| Q \| \gamma' J' >$ is the reduced matrix element and Γ_{ca} is the damping term between levels c and a. The factor $\Theta^{(K)}$ contains all the information about the angular dependence between the pump and Raman fields. Even though the summation in Eq. (1) extends over all the intermediate states, there are only three dominant terms in the case of thallium: those in which the intermediate states are $8s\ ^2S_{1/2}$, $6d\ ^2D_{3/2}$ and $7d\ ^2D_{3/2}$. The value of the reduced matrix elements is obtained through their relationship to the oscillator strength:

$$< \gamma J \|Q\| \gamma' J' >^2 = \frac{3\hbar e^2}{2m}\,\frac{(2J+1)\,f_{\gamma J - \gamma' J'}}{\Omega_{\gamma' J' \gamma J}} \qquad (2)$$

The oscillator strengths for p to s and p to d transitions have been calculated by Anderson et al,[8] and have also been experimentally determined by

(8) Anderson, E.M., Anderson, E.K., and Trusov, V.F., Opt. Spectr. (U.S.S.R.) 20, 471 (1966).

Gallagher and Lurio.[9] The signs of the matrix elements are determined from the work of Vriens[10] who used a combination of experimental and theoretical results to deduce these for indium and thallium. The angular dependence factor $\Theta^{(K)}$ for the Raman process has been calculated by Yuratich and Hanna.[7] For our purposes, we shall assume that both the pump and Raman fields are linearly polarized and for this case, we have

$$\Theta^{(0)} = \frac{1}{3} \cos^2 \beta \tag{3a}$$

$$\Theta^{(1)} = \frac{1}{2} \sin^2 \beta \tag{3b}$$

$$\Theta^{(2)} = \frac{1}{6} (3 + \cos^2 \beta) \tag{3c}$$

where β is the angle between the pump and Raman fields.

The stimulated Raman emission cross section σ_{SRE} i.e., related to the Raman susceptibility χ_r by

$$\sigma_{SRE} = \frac{-12\pi^2 i \epsilon_o}{\lambda_r} \left(\frac{8\pi \times 10^7}{c} I_p\right) \chi_r \tag{4}$$

where I_p is pump intensity in watts/cm^2 and λ_r is the wavelength of the Raman radiation. The calculated σ_{SRE} at the three Raman wavelengths 3083 Å, 1.649 μ and 1.975 μ (when the atom goes respectively to 6p $^2P_{3/2}$, 7p $^2P_{1/2}$ and 7p $^2P_{3/2}$ states) are respectively

$$\sigma_{SRE}\,(6p\ ^2P_{3/2}) = 1.72 \times 10^{-28} \frac{I_p}{\tilde{\Gamma}_{ca}},\ \text{cm}^2 \tag{5a}$$

$$\sigma_{SRE}\,(7p\ ^2P_{1/2}) = 3.40 \times 10^{-27} \frac{I_p}{\tilde{\Gamma}_{ca}},\ \text{cm}^2 \tag{5b}$$

$$\sigma_{SRE}\,(7p\ ^2P_{3/2}) = 1.38 \times 10^{-26} \frac{I_p}{\tilde{\Gamma}_{ca}},\ \text{cm}^2 \tag{5c}$$

(9) Gallagher, A., and Lurio, A., Phys. Rev. 136 A, 87 (1964).
(10) Vriens, L., Opt. Commun. 11, 396 (1974).

where $\tilde{\Gamma}_{ca}$ is in cm^{-1}. The line width is taken to be the same in all three cases since the dominant width is the pumping laser width (~ 100 cm^{-1}), natural and doppler widths being much less than 1 cm^{-1}. The largest stimulated emission cross-section is for the $6p\ ^2P_{1/2} \rightarrow 7p\ ^2P_{3/2}$ transition and thus ν_2 is expected to be ~ 5064 cm^{-1}.

C. PHASE MATCHING FOR THE FOUR-WAVE PROCESS

In any parametric process where the atomic state of the system remains unchanged during the nonlinear optical conversion process, both momentum and energy of the photons have to be conserved. In the four wave down conversion, this means that efficient down conversion will be achieved only if the $\vec{k}$ vectors of the three converted waves add up to the $\vec{k}$ vector of the KrF pump wave. Since we are dealing with near resonant down conversion it may be possible to phase match either intrinsically or by the addition of buffer gas in the right proportion. The former method is to be preferred if it is possible since it reduces the complexity of generating the right phase matching condition.

In the case of intrinsic phase matching, again two possibilities exist. In the first case, the frequency ν_4 is adjusted to produce the correct amount of dispersion so that all waves propagate collinearly. This may be possible because of the large dispersion of the electromagnetic wave at ν_4 near an atomic resonance. In the second case, the intrinsic phase matching can be achieved by having the wave vectors $\vec{k}_2$, $\vec{k}_3$, and $\vec{k}_4$ corresponding to the frequencies ν_2, ν_3 and ν_4 respectively propagate at slight angles to each other such that their vectorial sum adds up to the pump wavevector $\vec{k}_1$. Obviously, this can be done only when the algebraic sum of k_2, k_3 and k_4 is larger than k_1. In a lossy medium the wave number k is larger than

the free space wave number at frequencies slightly below a resonant frequency. In the case of KrF laser down conversion in thallium angle phase matching should therefore be possible for ν_4 chosen to be less than the $6p\ ^2P_{1/2}$ to $7s\ ^2S_{1/2}$ transition energy (26477 cm^{-1}).

An important point that is to be considered in phase matching is the real absorption of waves generated at ν_4 by the medium. The closer ν_4 is to a resonance, the larger is the absorption; $\chi^{(3)}$ is also larger near a resonance. However, the absorption coefficient in the wings of a Lorentzian line decreases, as $(\Delta E)^{-2}$, while $\chi^{(3)}$ decreases as $(\Delta E)^{-1}$. Hence, ν_4 should be chosen to minimize absorption while keeping $\chi^{(3)}$ reasonably high. For the case of thallium, collinear intrinsic phase matching seems possible only where ν_4 is less than 1 cm^{-1} from the $6p \rightarrow 7s$ resonance transition; unfortunately, absorption at this frequency is expected to be very large. It is therefore not a good operating point for the down converter. Noncollinear angle phase matching is therefore considered below for thallium.

The refractive index, $n(\nu)$, at a frequency ν is given by the Sellmeier equation[11]

$$n = \frac{kc}{\omega} = 1 + \frac{r_e}{2\pi} \sum_{i,j} \frac{N_i f_{ij}}{\left[\nu_{ij}^2 - \nu^2\right]}, \qquad (6)$$

where

r_e = 2.818 x 10^{-13} cm

f_{ij} = oscillator strength of the i-j transition

ν_{ij} = energy difference between i and j levels in cm^{-1}

N_i = number density of particles in the i^{th} level

(11) Miles, R.B., and Harris, E.E., I.E.E.E. - J.Q.E., QE-9, 470 (1973).

Equation (6) is only valid far from any resonance; i.e., when $|\nu - \nu_{ij}|$ is at least 5 or 10 times the width of the line at ν_{ij}. Using f_{ij} values from Ref. 8, N_i from the vapor pressure curve of Nesmeyanov[12] and ν_{ij} values from the tables of Moore,[13] the wave number k at any frequency $\nu (= \omega/2\pi c)$ can be calculated as a function of medium temperature when thallium vapor is in equilibrium with the liquid phase at that temperature.

For phase-matching the following two equations have to be satisfied:

$$(k_4 + k_3) \cos \Theta + k_2 \cos \phi = k_1 \tag{7}$$

and

$$(k_4 + k_3) \sin \Theta = k_2 \sin \phi , \tag{8}$$

where Θ and ϕ are the angles that $\vec{k}_3$ and $\vec{k}_2$ make with respect to pump field $\vec{k}_1$ (Figure 5). In the above, it is assumed that $\vec{k}_3$ is parallel to $\vec{k}_4$. This is not a necessary condition for phase matching, but it gives the smallest angle Θ. Also the roles of $\vec{k}_2$, $\vec{k}_3$ and $\vec{k}_4$ can be arbitrarily interchanged. The initial generation of photons at ν_2 takes place due to the Raman process and ν_2 can come at any angle. The direction Θ can therefore be chosen preferentially by making a cavity at frequency ν_2 and making the KrF beam come at an angle to the axis of the cavity. This was the reason for choosing k_1 and k_2 noncollinear. In Figure 6, ϕ is plotted as functions of output wave number ν_4 at different vapor temperatures. The precise operating point on this curve is chosen by maximizing the conversion efficiency and minimizing the absorption. These will be discussed more fully in the next two sections.

(12) Nesmeyanov, An. N., Vapor Pressure of the Elements (Academic Press, N.Y. 1963).

(13) Moore, C.E., Atomic Energy Levels, Vol. III, (N.B.S. circular 467, Washington, D.C., 1958).

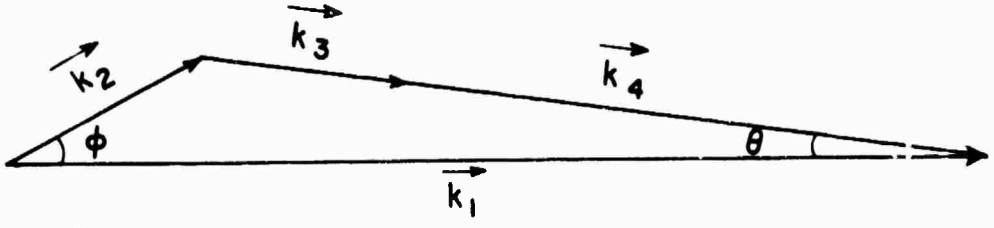

Figure 5 Schematic of Phase Matching

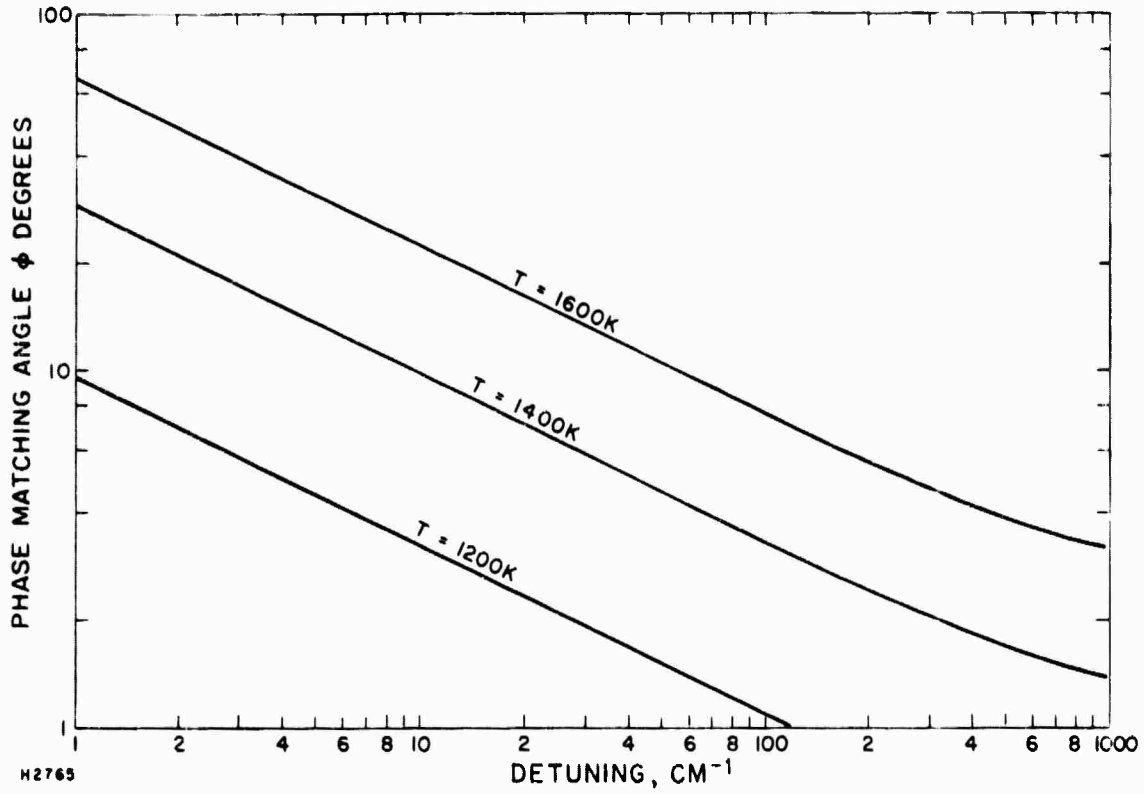

Figure 6 Phase-Matching Angle vs Output Wavenumber in Thallium

D. THE THIRD-ORDER NONLINEAR SUSCEPTIBILITY

Having identified the likely output wavelengths, we are now in a position to calculate the third-order nonlinear susceptibility for the four wave down conversion. The third-order nonlinear susceptibility $\chi^{(3)}(\omega_i; \omega_2, \omega_3, \omega_4)$ if given by[7]

$$\chi^{(3)} = -\frac{1}{6\hbar^3 \epsilon_o} S_T \sum_{J_1, J_2, J_3} \sum_{K} \frac{(-1)^{3J + K + J_2} (2K + 1)^{1/2}}{(2J + 1)}$$

$$< J \| Q \| J_1 > < J_1 \| Q \| J_2 > < J_2 \| Q \| J_3 > < J_3 \| Q \| J >$$

$$\begin{Bmatrix} J & K & J_2 \\ 1 & J_1 & 1 \end{Bmatrix} \begin{Bmatrix} J & 1 & J_3 \\ 1 & J_2 & K \end{Bmatrix} F(K) \qquad (9)$$

where

$$F(K) \equiv \frac{(((\epsilon_1^* \times \epsilon_2)^{(K)} \times \epsilon_3)^{(1)} \times \epsilon_4)_o^{(0)}}{(\Omega_{JJ_1} + \omega_2 + \omega_3 + \omega_4)(\Omega_{JJ_2} + \omega_3 + \omega_4)(\Omega_{JJ_3} + \omega_4)}$$

and S_T is the overall permutation operator indicating that the expression following it is to be summed over all permutations of the pairs $\epsilon_1\omega_1$, $\epsilon_2\omega_2$ etc. ϵ_i is the polarization vector for the i^{th} wave. It is easy to show that for $K = 1$, $F(K) = 0$ if all the waves are linearly polarized and thus only the cases $K = 0$ and $K = 2$ have to be considered. If we define a frequency factor $D^{-1}(J_1, J_2 J_3) \equiv F(K)$ with numerators put equal to unity, it is found that

$$F(0) = \frac{1}{3} D \qquad (10)$$

$$F(2) = \frac{2}{3\sqrt{5}} D \qquad (11)$$

It is now a simple matter to estimate $\chi^{(3)}$ for the parametric down conversion process.

The dominant terms are when $\gamma J = 6p_{1/2}$ $\gamma_1 J_1 = 8s_{1/2}$ or $7d_{3/2}$ or $6d_{3/2}$ $\gamma_2 J_2 = 7p_{1/2}$ or $7p_{3/2}$, and $\gamma_3 J_3 = 7s_{1/2}$. There are thus six dominant terms in the summation in Eq. (9). The only unknown in Eq. (9) then are the phases of the reduced matrix elements. These are obtained from the theoretical and experimental information about the phases of the radial matrix elements available in the literature[10, 14] and using an LS or jj - coupling scheme to relate the radial matrix elements to the reduced matrix elements. The resonant denominator D in $\chi^{(3)}$ contains three terms $\Delta\nu_1$, $\Delta\nu_2$ and $\Delta\nu_3$. The value of $\Delta\nu_1$ can be readily calculated knowing the KrF wavelength and the energy level of the first intermediate state. $\Delta\nu_2$ is actually equal to the width of the Raman line initially generated and can be taken equal to the width of the KrF laser pump. $\Delta\nu_3$ is a variable such that phase matching condition can be satisfied while keeping the absorption at the frequency ν_4 to a minimum. The estimated $\chi^{(3)}$ from Eq. (9) for thallium atom is given by

$$\chi^{(3)} \simeq (1.7 \times 10^{-29} + 5.1 \times 10^{-26}/\Delta\nu_2)/\Delta\nu_3 \text{ e.s.u.} \qquad (12)$$

where $\Delta\nu_2$ and $\Delta\nu_3$ are in cm^{-1}. For a KrF laser that is not narrowed, the line width is $\sim 100\ cm^{-1}$, while one whose line is narrowed with an etalon for example may be $\sim 10\ cm^{-1}$. Taking $\Delta\nu_2$ to be $100\ cm^{-1}$, we get,

$$|\chi^{(3)}| \simeq 5.3 \times 10^{-28}/\Delta\nu_3, \text{ e.s.u./atom} \qquad (13)$$

(14) Fano, V. and Cooper, J.W., Rev. Modern Phys. 40, 441 (1968).

The absorption cross section in line center is given by

$$\sigma_o = \pi r_e f/\Delta\nu \tag{14}$$

where $\Delta\nu$ is the width of the line in cm^{-1}. For the $6p_{1/2} \rightarrow 7s_{1/2}$ transition in thallium, the natural width is $\sim 2 \times 10^{-3}$ cm^{-1}, the doppler width at 1800 K is $\sim 2 \times 10^{-2}$ cm^{-1} and collision broadened width at 1 atm is ~ 0.2 cm^{-1}. Taking the collision broadened width for $\Delta\nu$, we find the absorption cross section in line center to be $\sim 5.5 \times 10^{-13}$ cm^2. Since the natural line is Lorentzian, the absorption cross section at a frequency tuned $\Delta\nu_3$ cm^{-1} away from line center can be calculated from $\sigma_o (\Delta\nu_c/2\Delta\nu_3)^2$. Thus for $\Delta\nu_3 \sim 200$ cm^{-1}, the absorption cross section is $\sim 1.4 \times 10^{-19}$ cm^2. The third-order nonlinear susceptibility at this detuning frequency is about 2.6×10^{-30} e.s.u./atom. It will be shown later that for thallium, this choice of $\Delta\nu_3$ produces a reasonable optimum of having large $\chi^{(3)}$ and tolerable absorption at the output frequency. In the following section, we solve the coupled nonlinear equations for the evolution of the field amplitudes taking into account absorption. The density of parametric medium necessary and its length for efficient conversion is also calculated.

E. CONVERSION EFFICIENCY

The coupled amplitude equations describing the parametric four-wave conversion process are

$$\frac{dA_1}{dz} = -\beta_1 A_2 A_3 A_4 - \alpha_1 A_1 \tag{15}$$

$$\frac{dA_2}{dz} = +\beta_2 A_1 A_3 A_4 \tag{16}$$

$$\frac{dA_3}{dz} = + \beta_3 A_1 A_2 A_4 \tag{17}$$

$$\frac{dA_4}{dz} = + \beta_4 A_1 A_2 A_3 - \alpha_4 A_4 \tag{18}$$

where A_j is the amplitude of the electric field of the jth wave, α_j is the linear absorption coefficient and β_j is the nonlinear coupling constant ($\beta_j = 3N k_j \chi^{(3)}/4n_j$). Only waves 1 and 4 are assumed to have absorption in the medium since they have resonance with the initial state of the atoms. It is not difficult to include absorption of the other two waves as well. It is convenient to rewrite the Eqs. (15) - (18) in a non-dimensional form with the help of the following substitutions:

$$y_j = \frac{A_j}{A_{10}} \sqrt{\frac{\omega_1}{\omega_j}} \tag{19a}$$

$$\zeta = \frac{z}{L} \tag{19b}$$

where A_{10} is the initial amplitude of the pump wave and L is the length of the nonlinear medium. The reduced equations are,

$$\frac{dy_1}{d\zeta} = - \beta y_2 y_3 y_4 - \gamma_1 y_1 \tag{20}$$

$$\frac{dy_2}{d\zeta} = + \beta y_1 y_3 y_4 \tag{21}$$

$$\frac{dy_3}{d\zeta} = + \beta y_1 y_2 y_4 \tag{22}$$

$$\frac{dy_4}{d\zeta} = + \beta y_1 y_2 y_3 - \gamma_4 y_4 \tag{23}$$

where

$$\beta = \frac{12\pi^2}{c\lambda_4}\left(\frac{\omega_2\,\omega_3}{\omega_1\,\omega_4}\right)^{1/2} I_{10}\, N\, L\, \chi^{(3)},$$

$$\gamma_1 = \alpha_1\, L \text{ and } \gamma_4 = \alpha_4\, L.$$

In the above I_{10} is the incident intensity of the pump wave and N is the density of the nonlinear medium. y_j^2 gives the normalized photon density in the jth mode and the conversion efficiency is given by y_4^2 since ν_4 is the output frequency of interest. Equations (20) - (23) can be solved exactly analytically in the absence of losses. The initial conditions are, $y_1 = 1$, $y_2 = \delta$, $y_3 = \Delta$ and $y_4 = 0$ at $\zeta = 0$. The analytical solution involves Jacobi's elliptic functions and the expression for the conversion efficiency η is given by

$$\eta = \frac{\Delta\ sn^2(u,\rho)}{\Delta + 1 - sn^2(u,\rho)} \tag{24}$$

where

$$u = \beta\left[\delta\,(1+\Delta)\right]^{1/2}$$

$$\rho = \left[\frac{\delta - \Delta}{\delta\,(1+\Delta)}\right]^{1/2}$$

It must be emphasized that the expression (24) is valid only for the case of no losses. Typical values of Δ and δ might be 10^{-3}. When $\delta = \Delta$, we have $\rho = 0$ and the Jacobian elliptic function sn u reduces to sin u. Complete conversion is obtained when sn u equals unity, which means $u \simeq \pi/2$. This implies that β should be equal to $\sim \pi/2\ \sqrt{\delta}$ for complete conversion. Figure 7 shows a plot of conversion efficiency vs β for typical values of δ and Δ. When we take into account the absorption of the waves, it is in general

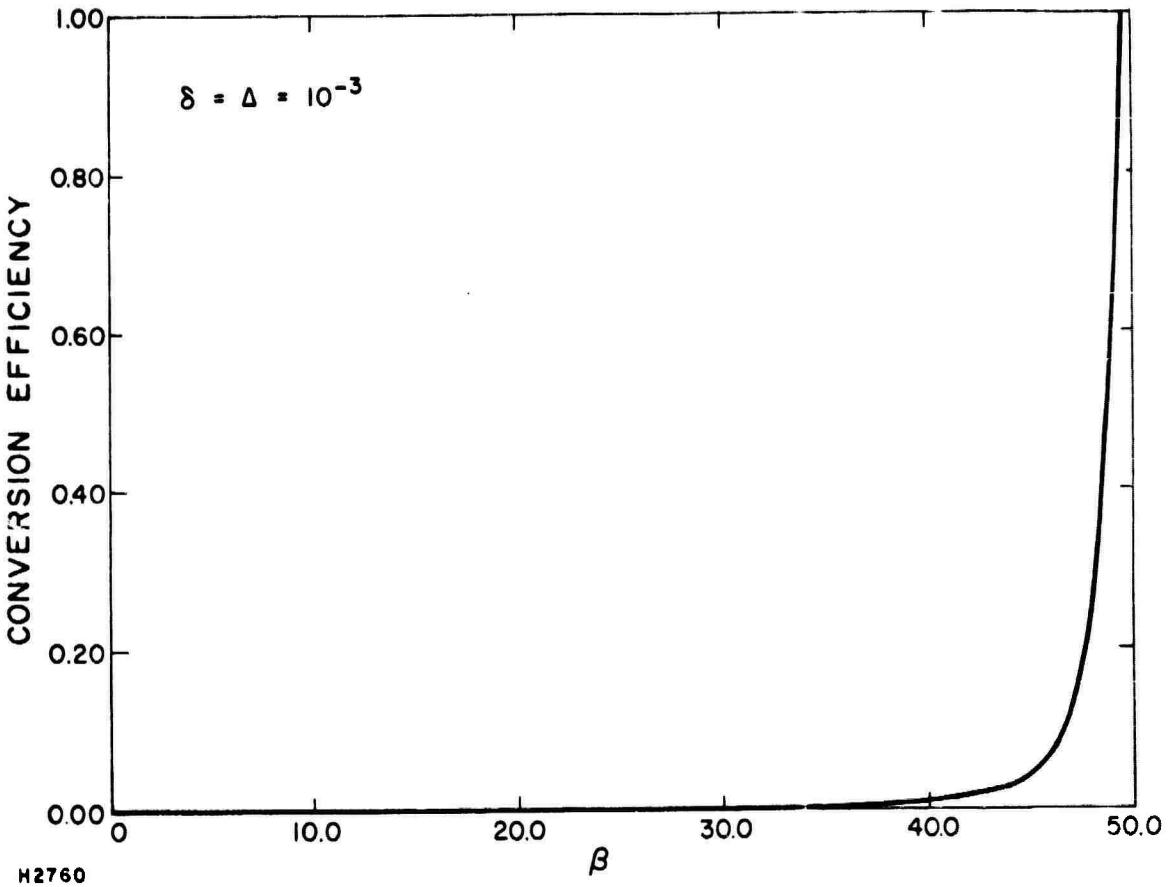

Figure 7 Conversion Efficiency vs β, $\gamma_1 = \gamma_4 = 0$

not possible to obtain closed form analytical solutions. Equations (20) - (23) are, however, easily solved in a computer. Figures 8 to 10 show typical results of such computer runs. It is evident from the figures that absorption at ν_4 affects the generated output much less than absorption of the pump wave. This is not surprising since the bulk of ν_4 is generated over a small length at the very end of the nonlinear medium while abosrption of ν_1 takes place over the entire length of the nonlinear medium.

For $\delta \simeq 10^{-3}$, we find that we need $\beta \simeq 50$ for efficient parametric conversion. If one of the three generated waves is initially created by the Raman process, the corresponding resonant denominator should be replaced by the pump laser linewidth. Thus for a diffraction limited pump laser, the conversion parameter β can be written as

$$\beta = \Lambda \, N \, P/\gamma_\ell \tag{25}$$

where P is the KrF laser power in watts, γ_ℓ is the laser linewidth in cm^{-1} and Λ is an effective cross section in cm^2/w. In the case when $\Delta\nu_1$ and $\Delta\nu_3$ are very small, the expression for $\chi^{(3)}$, is dominated by a single term, and Λ can be written as

$$\Lambda \simeq \frac{9}{4\pi^2} \frac{r_e^2}{\hbar c^2} \times 10^7 \frac{\left[(gf)_{01}\,(gf)_{21}\,(gf)_{32}\,(gf)_{03}\right]^{1/2}}{\Delta\nu_1 \, \Delta\nu_3}$$

$$\times \sum_K \frac{(2K+1)^{1/2}}{3(2J+1)} \begin{Bmatrix} J & K & J_2 \\ 1 & J_1 & 1 \end{Bmatrix} \begin{Bmatrix} J & K & J_2 \\ 1 & J_3 & 1 \end{Bmatrix}$$

$$\times \left\{ \delta_{K,\,0} + 2\delta_{K,\,2}/\sqrt{5} \right\} \tag{26}$$

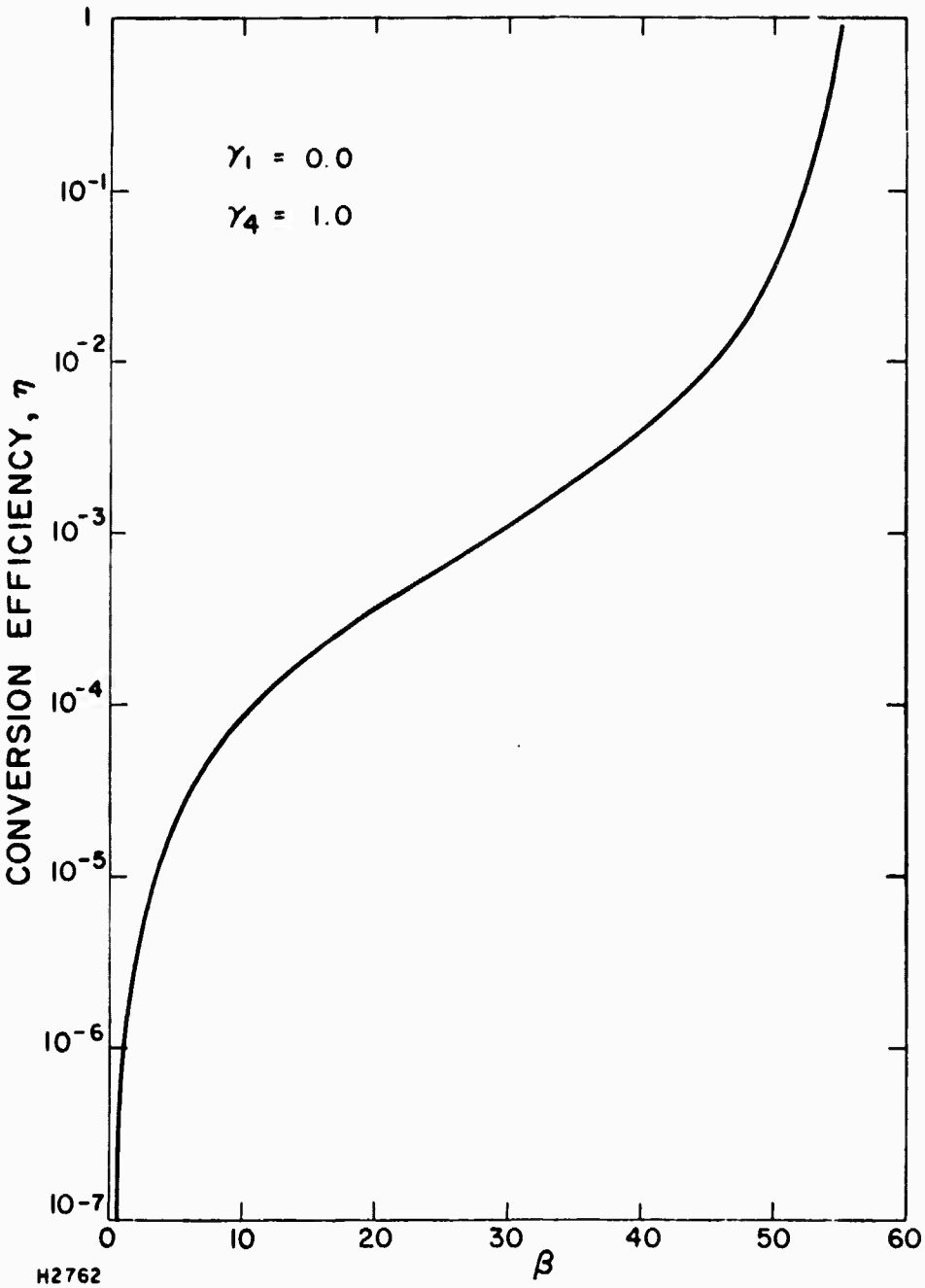

Figure 8 Conversion Efficiency vs β, $\gamma_1 = 0$, $\gamma_4 = 1$

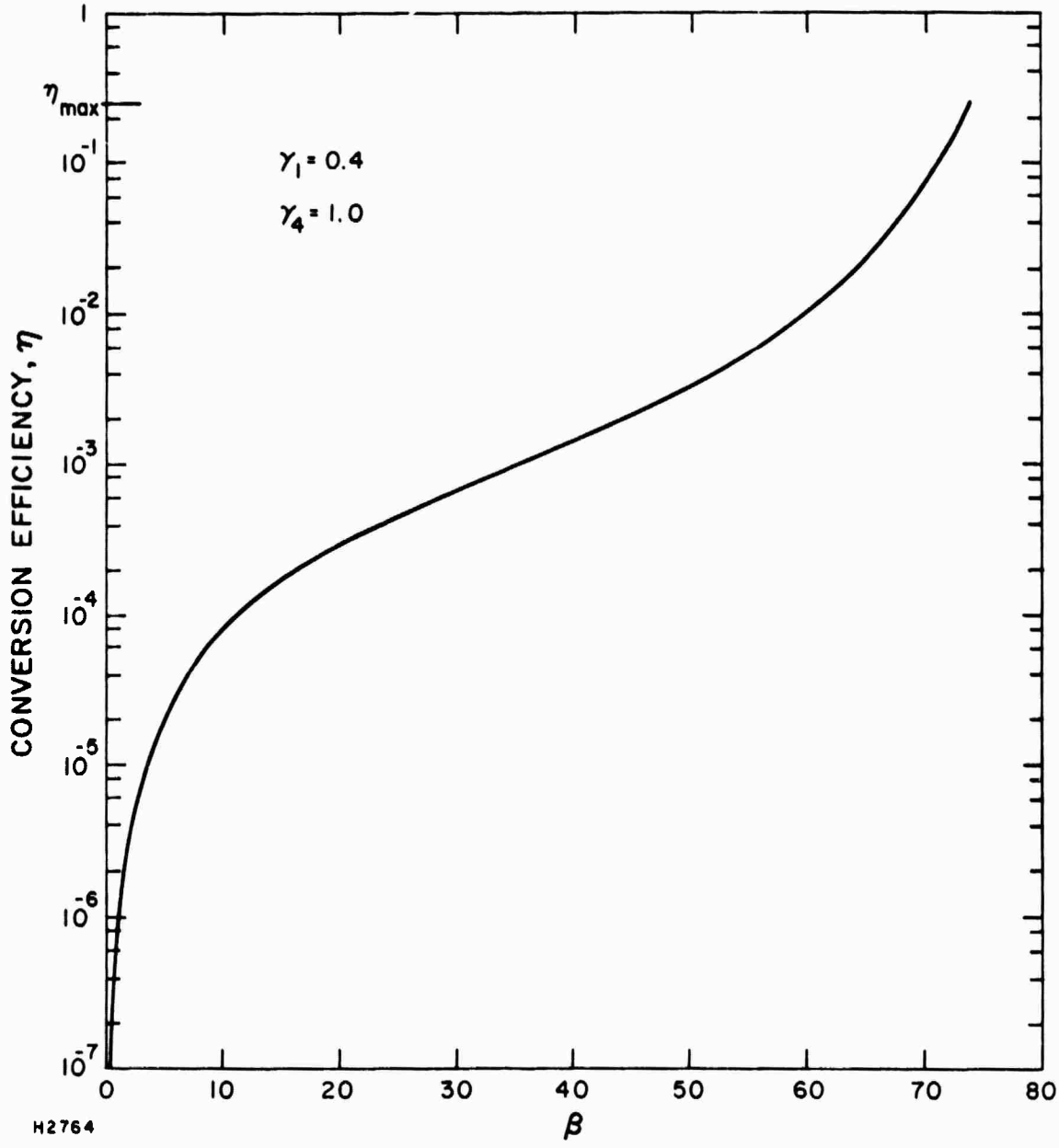

Figure 9 Conversion Efficiency vs β, $\gamma_1 = 0.2$, $\gamma_4 = 1$

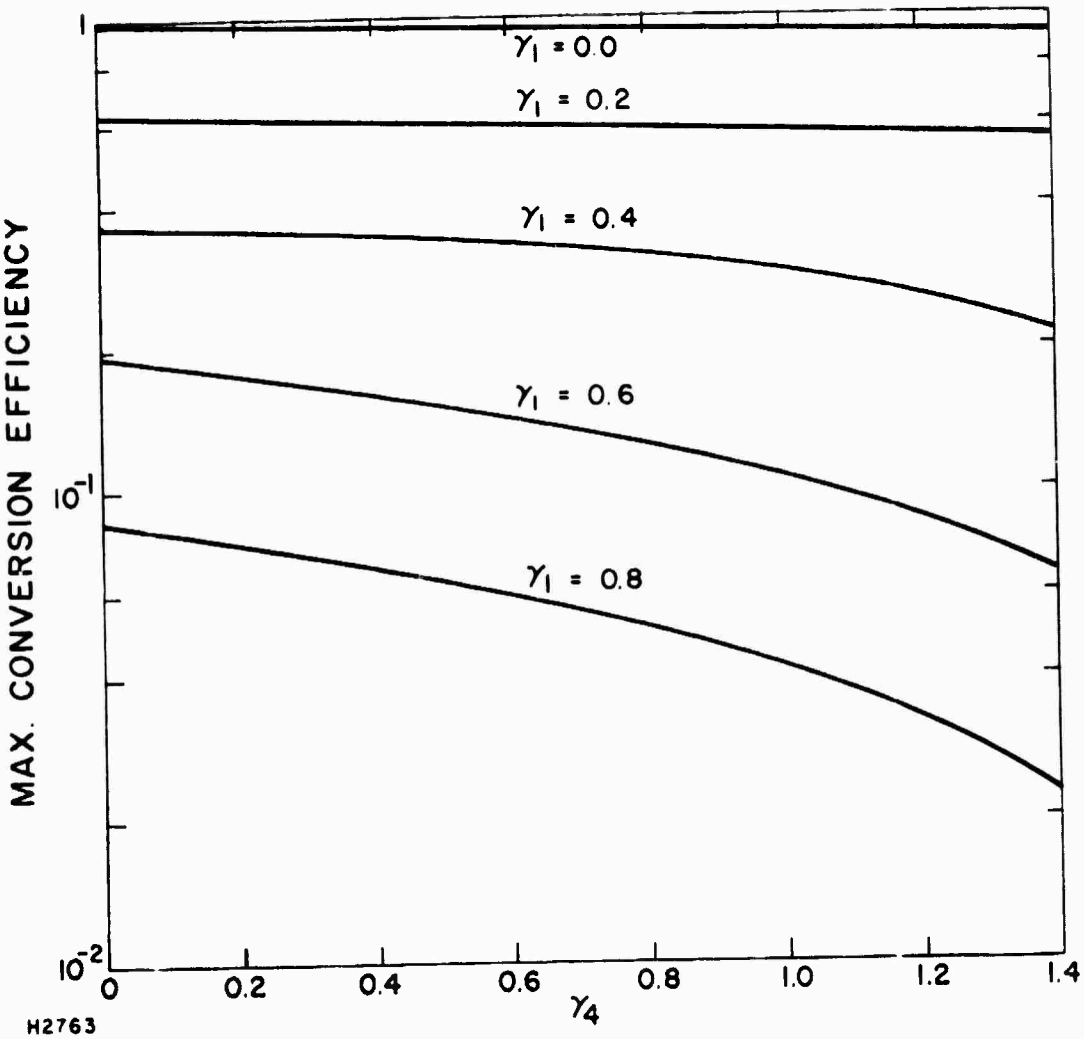

Figure 10 Max Conversion Efficiency vs γ_4

$$= 1.91 \times 10^{-13} \left[(gf)_{01}\,(gf)_{21}\,(gf)_{32}\,(gf)_{03}\right]^{1/2} \Delta\nu_1\ \Delta\nu_3\ (2J+1)$$

$$\times \sum_K \left(\delta_{K,\,0} + 2\delta_{K,\,2}\right) \begin{Bmatrix} J & K & J_2 \\ 1 & J_1 & 1 \end{Bmatrix} \begin{Bmatrix} J & K & J_2 \\ 1 & J_3 & 1 \end{Bmatrix}, \ \mathrm{cm}^2/\mathrm{W} \quad (27)$$

The quantity Λ is an atomic parameter for a set of given frequencies. In Figure 11 a map of constant P/γ_ℓ is plotted in the coordinates of Λ and N. Each atomic system is represented on this map by a horizontal line, whose position depends upon the density of the medium that may be produced in the gas phase at reasonable temperatures. The line of constant P/γ_ℓ have been plotted on the assumption that β equals 50. Three elements are plotted on this map. These are thallium, lithium and lead. From the map it is seen that both lithium and thallium are good parametric down conversion candidates from the point of view of ease of obtaining the operating density. However, both require angle phase matching for intrinsic phase matching. Colline phase matching conditions may be obtained by the addition of buffer vapor like mercury.

In the case of thallium an operating density of 10^{17} cm^{-3} over a path length of 100 cm will give an integrated absorption depth of ~ 1.4 which is acceptable for a down converter. This justifies our choice of $\Delta\nu_3$ ~ 200 cm^{-1} to keep $\chi^{(3)}$ reasonably large while the absorption cross section remains at a tolerable level.

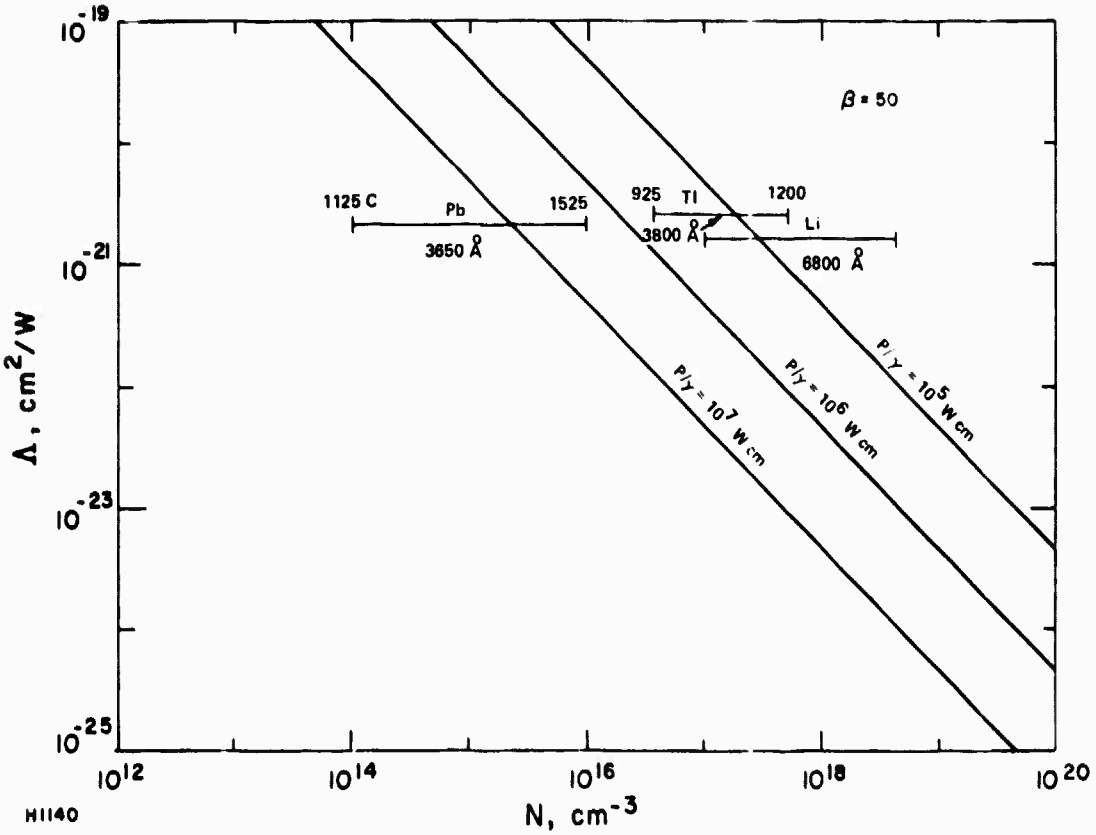

Figure 11 Map of Λ vs N for Certain Candidate Atoms Considered for the Parametric Down Conversion

THIS
PAGE
IS
MISSING
IN
ORIGINAL
DOCUMENT

III. EXPERIMENTS

A. INTRODUCTION

The successful demonstration of optical conversion in any laser system through stimulated Raman or Parametric conversion requires optimization of a number of variables to achieve reasonable gain, namely, overall system cross section, which is in turn influenced by the laser intensity, bandwidth and wavelength, and also the ability to produce sufficient densities of acceptor candidates to show reasonable conversion. We will describe the results and status of this program with regard to the stimulated Raman candidates in the next two sections and then describe how these systems were coupled to producing lasing in a couple of candidates in the section titled "Lasing Experiments."

B. ACCEPTOR CANDIDATE PRODUCTION

Under the early phases of this contract, the stimulated Raman and direct optical pumping cross sections for various candidates were calculated.[5] For the stimulated Raman process, the total gain, $g_o L$, for a single pass system is equal to $N\sigma_{SRE}L$, where N is the density of atoms and L is the active length of Raman medium. For a diffraction limited beam, the maximum value of the intensity-length product is equal to P/λ_p where P is the pump laser power and λ_p is the pump wavelength. Thus, $g_o L$ can be written as,

$$g_o L = \Lambda NP/\gamma_\ell \qquad (28)$$

where

$$\Lambda = 9.55 \times 10^{-14} \left(\frac{\nu_s}{\nu_{23}}\right) \frac{f_{12}(gf)_{32}}{(\Delta\nu)^2} \sum_{K=0}^{2} \begin{Bmatrix} J_3 & K & J_1 \\ 1 & J_2 & 1 \end{Bmatrix}^2 \Theta^{(K)} \text{ cm}^2/\text{W},$$

γ_ℓ is the bandwidth in cm^{-1}, and P is in watts. The quantity Λ is then an atomic parameter for a given pump wavelength and given pump and Raman field polarizations. In what follows, we shall assume for convenience, that both pump and Raman fields are linearly polarized and are traveling in the same direction.

In Figure 12, a plot of constant $g_o L$ is presented in the coordinates of Λ and N. Each atomic system is represented on this graph by a horizontal line, whose position depends upon the density of the medium that may be produced in the gas phase and extent represents the degree of uncertainty in experimentally achievable atom production. The lines of constant $g_o L$ have been plotted on the assumption that P/γ_ℓ of the pump laser equals 10^5 W cm. From this plot and the results of experiments we performed to produce the needed metal atom densities, using the techniques of flash photolysis or discharge dissociation of organo-metallics, we can conclude that for KrF down conversion, the most promising conversion systems, in terms of ease of demonstration of principle, are molecular hydrogen, atomic iron in the gas phase, and calcium vapor in a heat pipe. Although our proposal candidate, platinum, does not show as large a projected gain as does atomic iron, it has the advantage of potentially shifting the KrF output to more propagating wavelengths. One aspect many of these systems have in common is the effect of direct optical pumping as a competing process to near resonant or resonant Raman processes. It was useful,

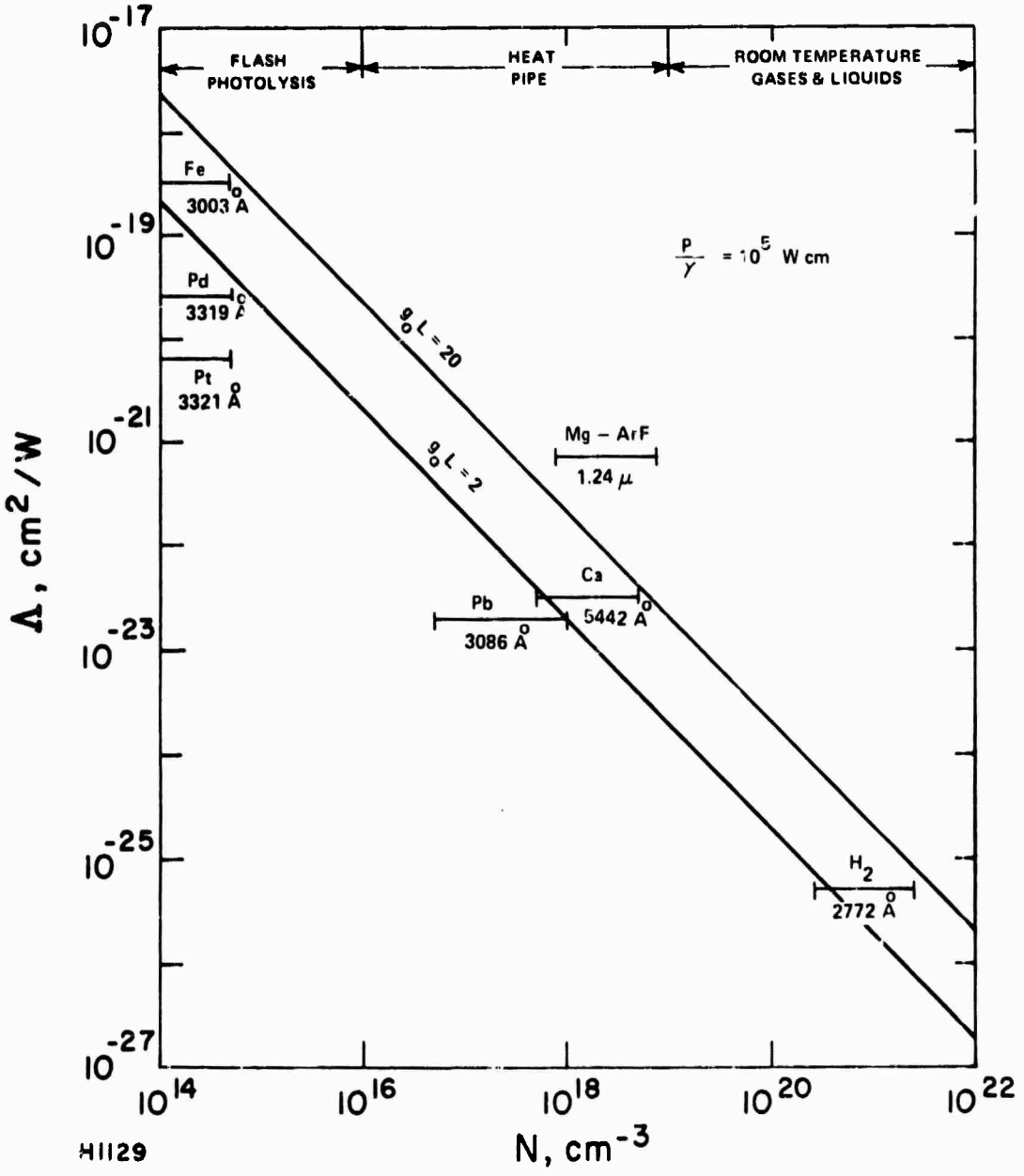

Figure 12 Anticipated Stimulated Raman Gain of Various Accepted Candidates

therefore, to consider these effects using iron as an example, since experiments with a glow discharge showed we could produce atomic iron densities in excess of 8×10^{13} atoms/cc using iron pentacarbonyl as the precursor. (This is equivalent to a thermal temperature near 1600 °K.) We were also able to generate significant densities of atomic iron by the flash photodecomposition of $Fe(CO)_5$ in a buffer of argon.

These calculations, which were summarized in our previous semi-annual report,[5] showed the anticipated gain for direct optical pumping was about 250 times greater than for the Raman process. We, therefore, had every expectation that the atomic iron system should efficiently convert the KrF pump radiation to longer wavelengths near 300 nm.

C. PUMP LASER SOURCES

It was the original premise of this experimental approach to use a double dye laser as the source to perform conversion experiments. This system would have the advantage of being spectrally narrow ($\Delta \lambda \sim 1$ Å near 248 nm) as well as tunable. After much difficulty, the vendor (Phase-R Corp.) was able to provide a tunable, flashlamp pumped dye laser utilizing Coumerin 504 dye (Exciton Corp.) and a cooled ADP crystal for frequency doubling (see Figure 13). Output was measured to be near 5 mJ in a 500 nsec pulse. This laser was found to be useful to perform absorption experiments of the organo-metallic/buffer gas photodecomposition/discharge dissociation mixtures to determine loss processes at the pump laser frequency. Referring to Figure 12, it can be seen that its output ($P/\gamma \sim 10^3$ Wcm) is not sufficient for many of these systems to be useful as a pump laser. It should be possible, however, to use it in a MOPA configuration to be amplified in a discharge laser device to provide somewhat tunable spectrally narrow, high power pulses.

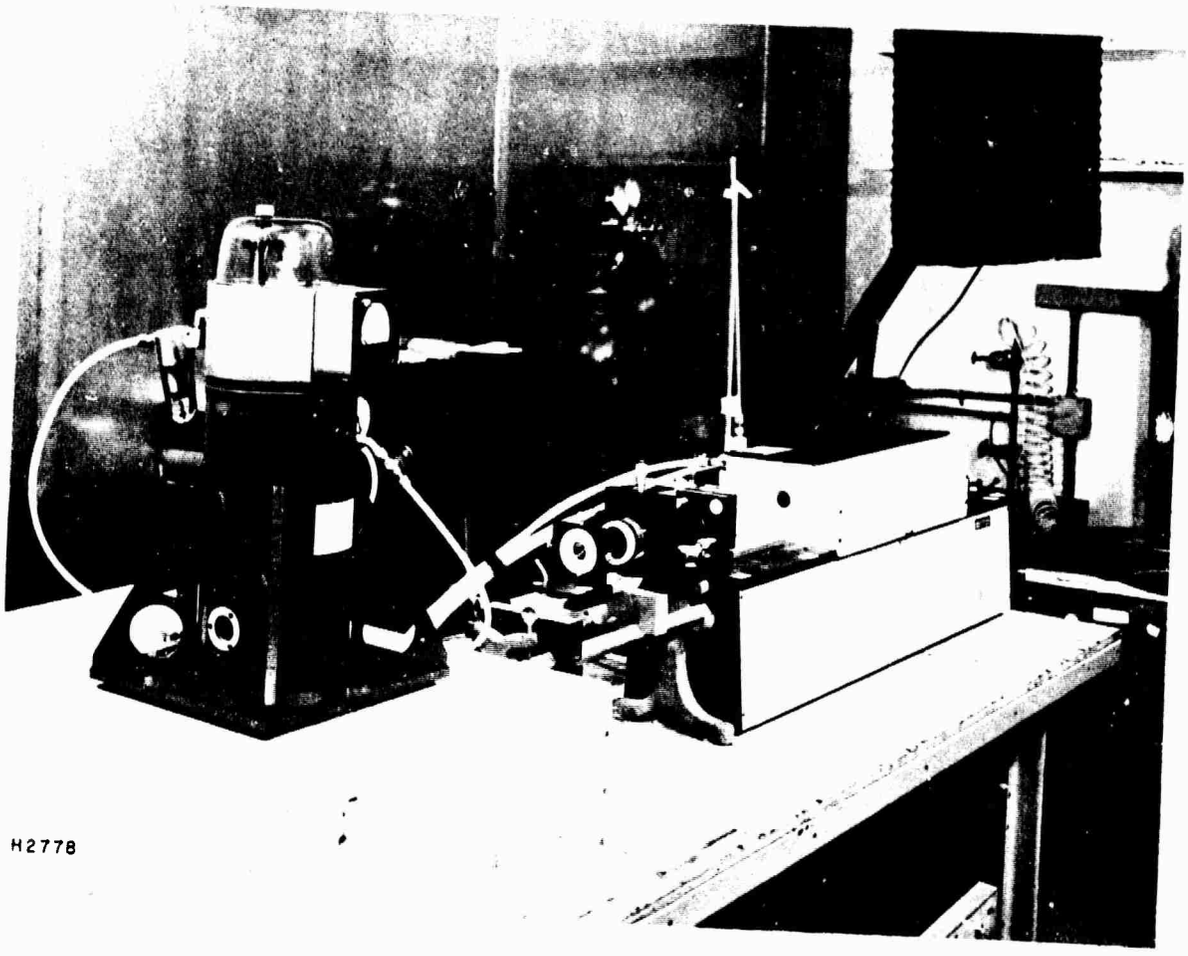

Figure 13 Doubled Dye Laser System

The conversion experiments were performed using a discharge initiated KrF excimer laser (Tachisto Corp., Needham, MA). As delivered, this laser provided approximately 50 mJ of output in a 20 nsec pulse with a stated beam divergence near 4 mrad. The output is a rectangle ~15 mm x 4 mm. To achieve values of P/γ as high as possible, it was necessary to improve the laser beam quality so it could be focussed tightly. This was accomplished using the technique described by Loree et al of LASL[4] and consisted of replacing the supplied output coupling mirror with a 50 cm plano-convex lens (suprasil). This provided an unstable cavity configuration of quite a good beam quality which focussed near 50 cm from the Tachisto exit port. Typical output was near 30-40 mJ in 20 nsec which, therefore, provided approximately 1-2 MW of power. One and two shot exposures of the output were analyzed to obtain the spectral width and it was found to be near 10 Å (~ 160 cm^{-1} fwhm). This suggests that for this pump laser a reasonable value for P/γ is 1-2 x 10^4 Wcm. Considerable improvement can be made by narrowing the bandwidth with subsequent increased ease of conversion demonstration (see Figure 12).

D. LASING EXPERIMENTS

1. Atomic Iron

As a check on our overall system, we opted to repeat the hydrogen conversion experiments of the LASL group[4] using a 60 cm stainless steel shock tube section filled to near 10 atm with hydrogen. We were able to observe 4 or 5 Stokes shifted lines as well as one anti-Stokes line using a simple prism spectrograph and polaroid film for observation. Satisfied with our laser's performance and implied beam quality, we then

attempted our best candidate in terms of ease of demonstration, i.e., atomic iron. We were able to show on our initial attempts, single pass amplified spontaneous emission near 300 and 304 nm (see Figure 14) using discharge dissociation of $Fe(CO)_5$ in 50 torr of neon to provide the required atomic iron density.[6] Subsequent spectra taken with a moderate resolution spectrograph showed that for high iron densities we were seeing output on four different lines (see Figure 15). The apparent doublet shape of the KrF laser pulse is real and is likely due to the presence of a strong absorber in the discharge cell. By superimposing some atomic mercury spectra onto these type of data, we were able to correlate our observations of wavelength with the known[15] transitions in the atomic iron system to confirm the origin for these lasing lines. These conclusions are summarized in Figure 16. We were able to delay the time the KrF pump laser fired relative to the discharge and, thereby, probe the spectral output variation with the decaying atomic iron density. The intensities of the various lines were then probed through densitometer traces of the photographic plate. These data are plotted as intensity peak height in arbitrary units vs time on a semi-logarithmic scale (see Figure 17). From these data, it is readily seen that the 300 nm transition shows the greatest output and persists with decreasing iron density due to its higher total gain in agreement with theoretical calculations.

In addition to doing spectrally resolved measurements, we performed experiments with calibrated photodiodes to establish temporal characteristics and measure overall conversion efficiency (see

(15) Corliss, C. H. and Bozman, W. R. NBS Monograph 53 (1962).

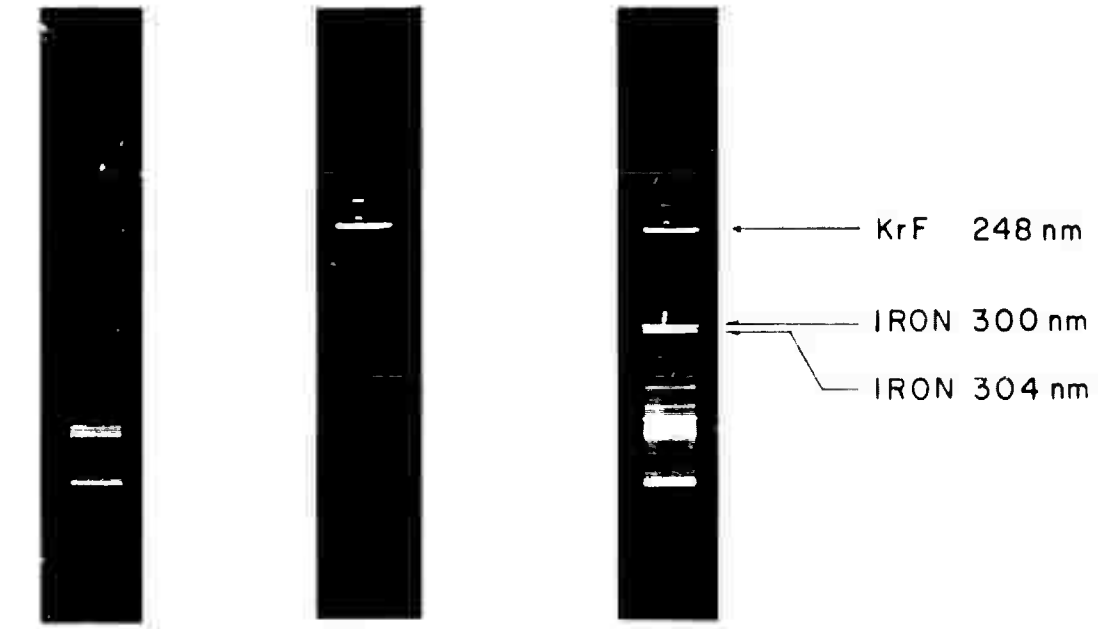

Figure 14 Atomic Iron Laser

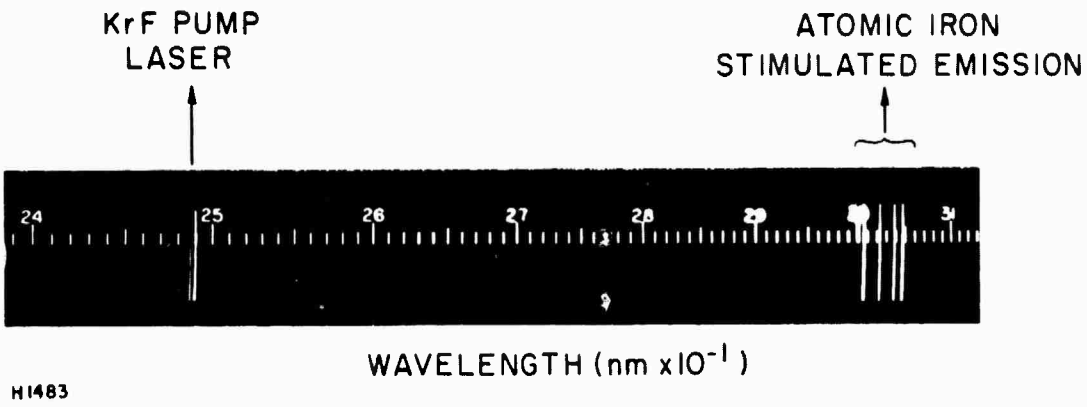

Figure 15 Optically Pumped Atomic Iron Laser

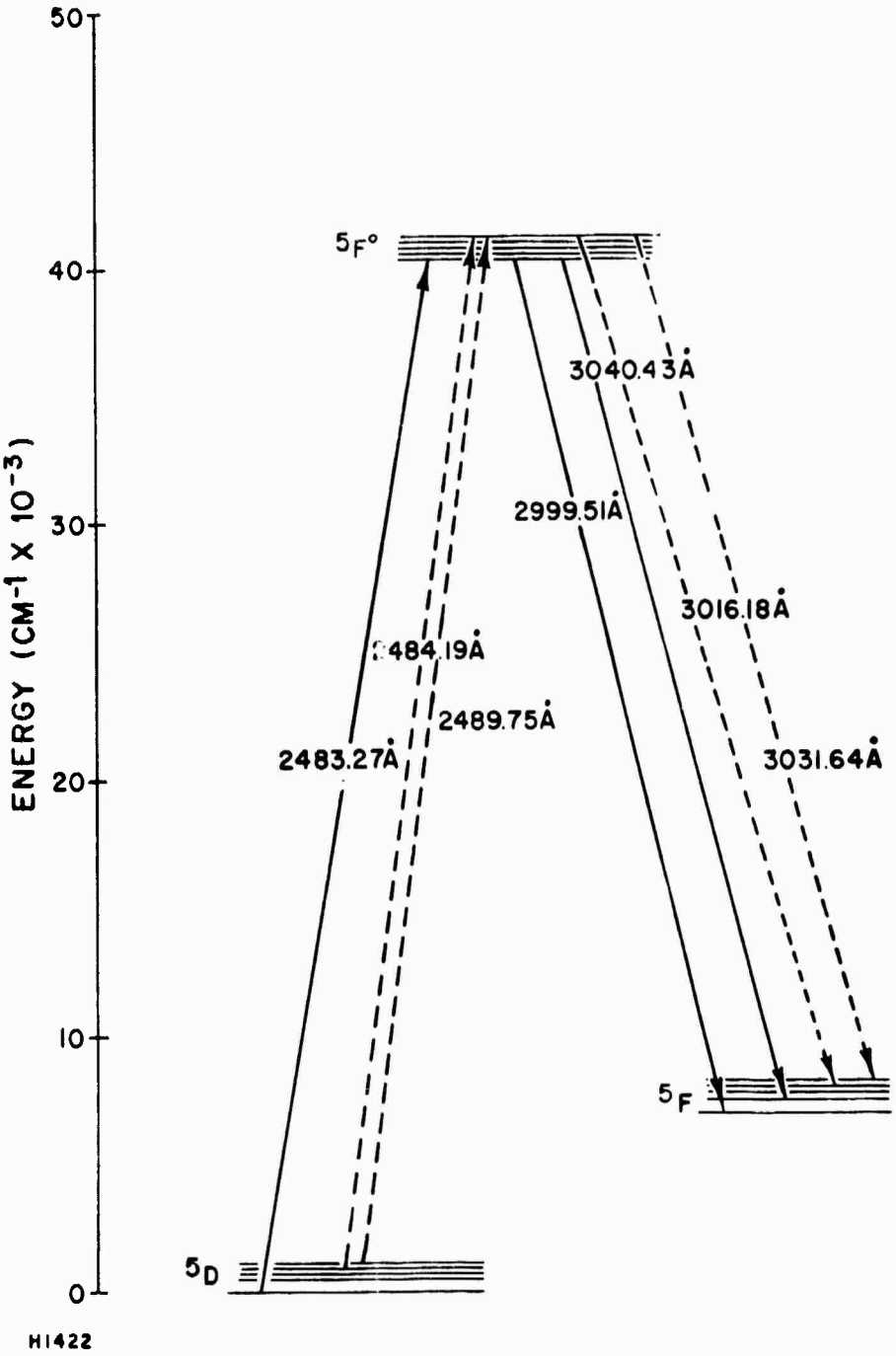

Figure 16 Atomic Iron Lasing Transitions

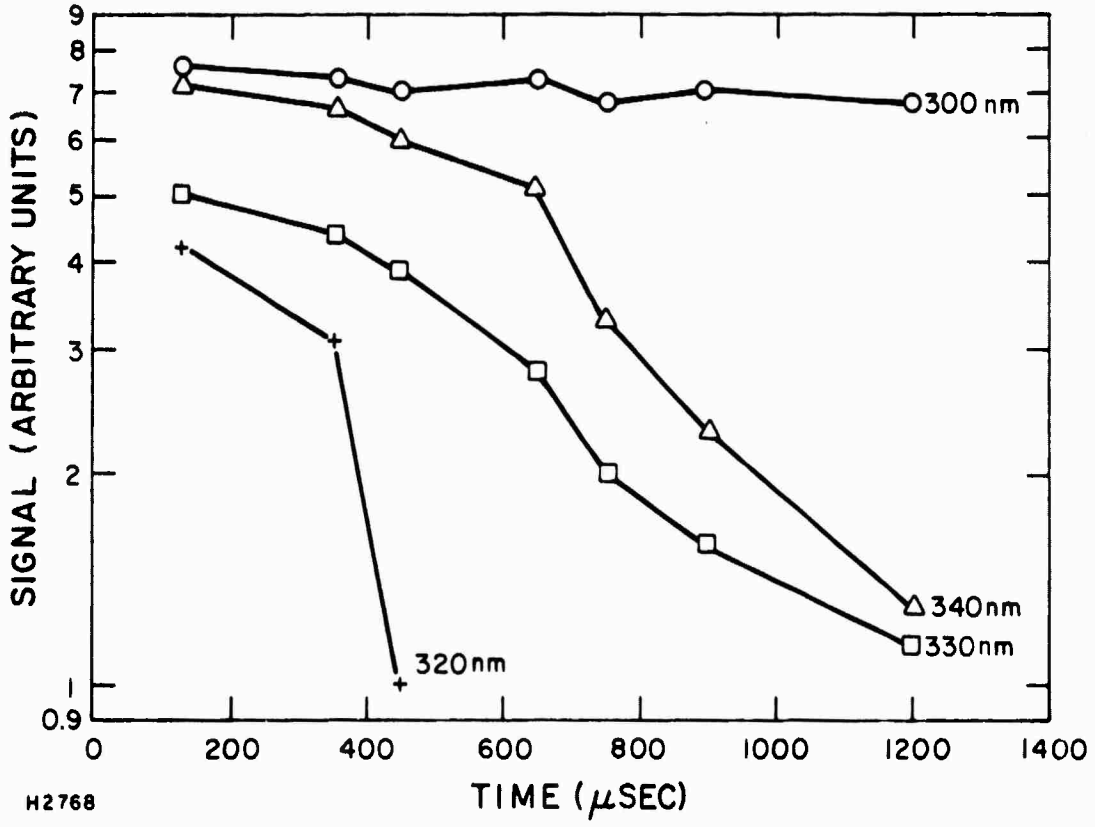

Figure 17 Spectral Distribution as a f (Atomic Iron Density)

Figure 18). As can be seen from the figure, we could also measure simultaneously, through atomic absorption techniques using an iron hollow cathode, the production and decay of the various iron states produced in the discharge cell. The shot to shot output of the KrF pump laser was also monitored by an additional photodiode. Typical data are shown in Figure 19.

From the absorption information, it can be seen that the maximum density of atomic iron in the lowest spin-orbit state ($^5D_4$) is observed at times near 300 μsec after the initiation of the discharge. Any direct discharge production must occur on a faster time scale (see Figure 20). This additional iron atom production beyond the off time of the discharge probably arises from energy transfer reactions and radical reactions as well as cascading of higher lying excited states of iron into the lowest energy state. From the work of Callear and Oldman[16], it is likely that the J = 0, 1, 2 and 3 levels of the ^5D state under our experimental conditions quickly (100 μsec) establish a Boltzmann distribution, then as a group decay into equilibrium with the $^5D_4$ state. The characteristic time of this latter process varies with the nature of the quenching gas present. For 50 torr of neon, its likely to be of the order of several msec, whereas hydrogen was measured to relax these states with a rate constant of $7.4 \pm 0.7 \times 10^{-12}$ cm^3/sec. By adding 3 torr of hydrogen to the 50 torr of neon, we observed increased laser output at earlier times probably at 300 and 304 nm and at the expense of the 320 or 330 nm. Also, data showing the time for peak signal (see Figure 21) coincide closely with the atomic absorption data shown in Figure 19, supporting the induction time for optimum iron production.

(16) Callear, A. B. and Oldman, R. I. Trans. Far. Soc. 63, 2888 (1967).

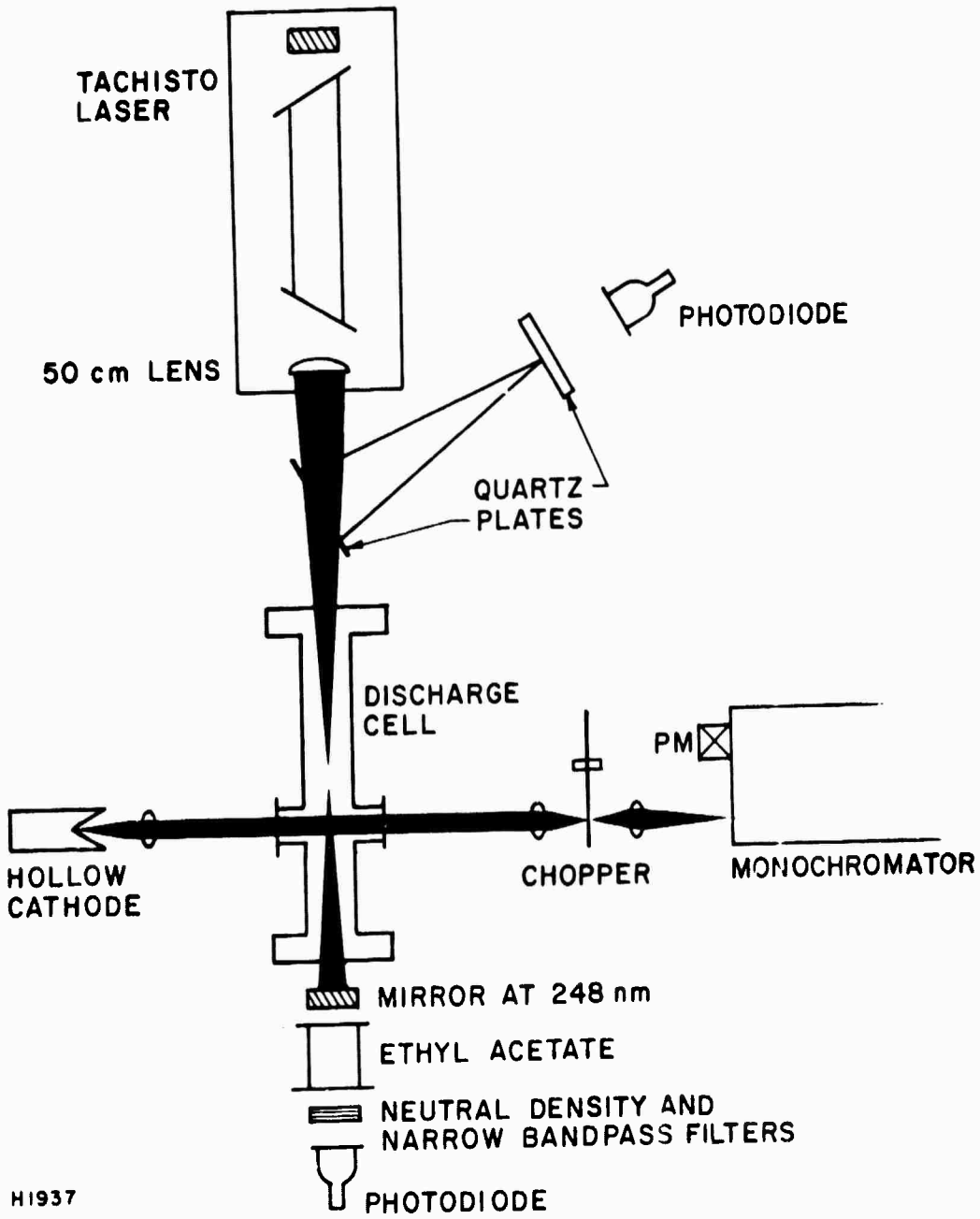

Figure 18 Experimental Approach

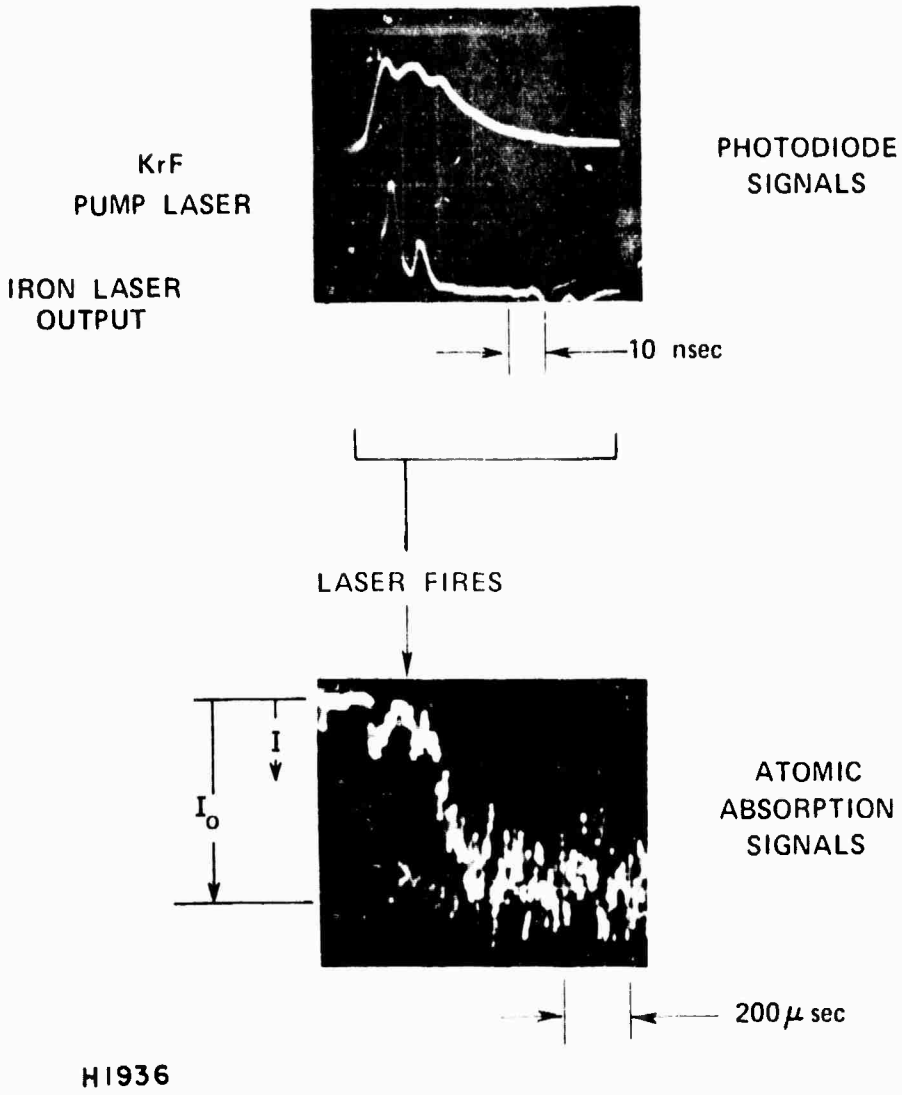

Figure 19 Experimental Data

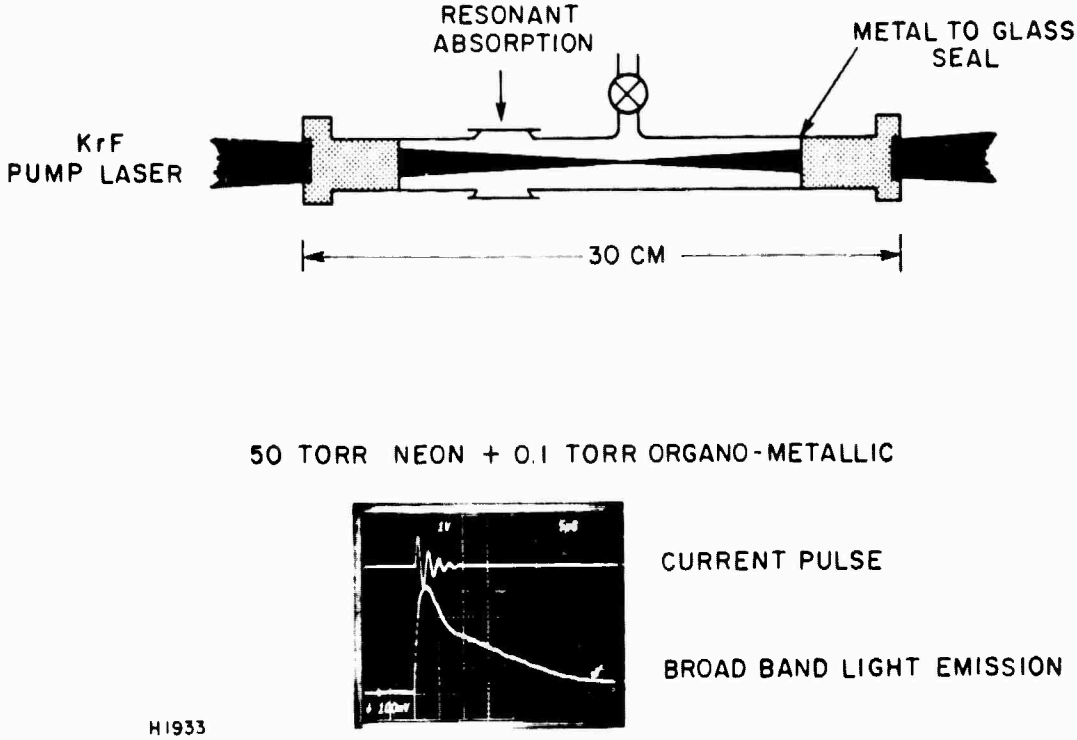

Figure 20 Discharge Cell Characteristics

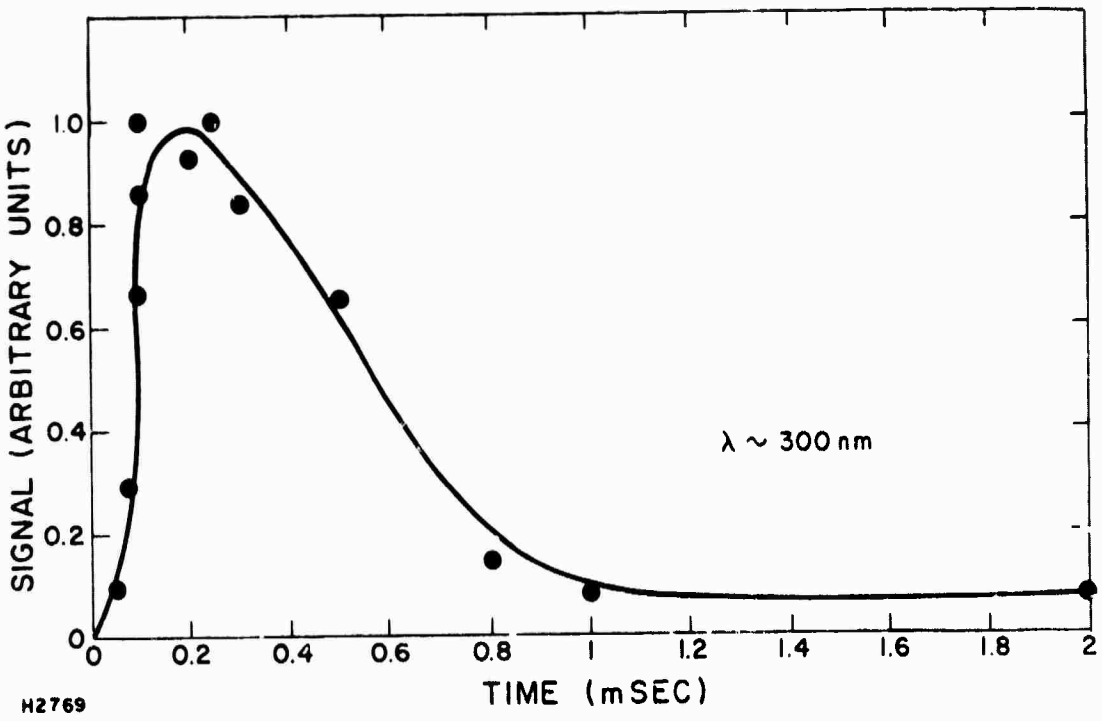

Figure 21 Converted Laser Output vs Atomic Iron Density

In addition to showing conversion of KrF with atomic iron produced in a discharge, we were able to demonstrate lasing with iron produced by the photodecomposition of $Fe(CO)_5$ in a buffer of Ar. In contrast to the discharge, we saw prompt iron atom production (see Figure 22) and therefore chose to fire the laser at times near 40 μsec after the flash initiation. The flashlamp temporal behavior is such that it exhibits a fwhm of nearly 8 μsec and a time to 98% extinction of approximately 40 μsec. Since we routinely produced more iron atoms in the discharge than in the flash (e.g., 4×10^{12} vs 3×10^{11} atoms/cc), we observed higher conversion efficiency in the discharge method. These data suggest that for the higher iron densities, we demonstrated overall conversion efficiency of 1-2%. This is in complete agreement with our expectations. As discussed in our proposal, to produce higher conversion efficiency with these refractory candidates, one must recycle the atoms during the KrF laser pulse time scale, i.e., return the lower laser level population to the initial state through collisions with an efficient quenching gas for subsequent re-excitation by the laser field (see Figure 23). In that the pump laser used in these experiments had a 20 nsec pulse, it is difficult to demonstrate this effect. By adding sufficient quenching gas to relax on a time scale fast compared to 20 nsec, the likelihood of competing unfavorably with the spontaneous emission lifetime ($\sim$ 2 nsec) is assured whereas any scaleup KrF laser system is projected to have pulse lengths of order 1 μsec and the recycling time requirement is thereby significantly reduced. We did, however, investigate the effect of some of the quenching candidates on the flash production of iron. These results are shown in Figure 24. These data are interpreted as evidence that the initial production of iron atoms is not significantly affected by the

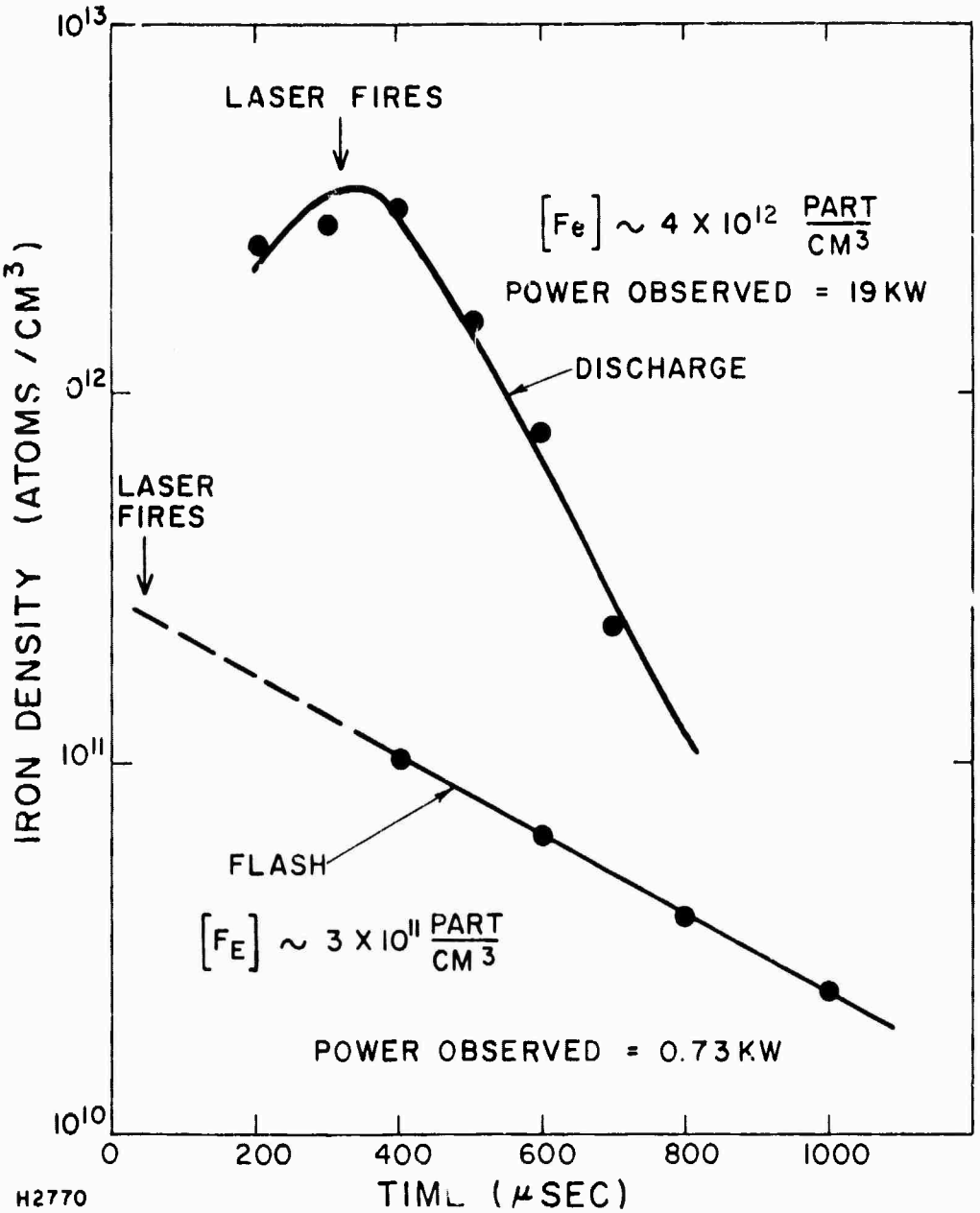

Figure 22 Flash vs Discharge: Iron Laser Output

- MECHANISM

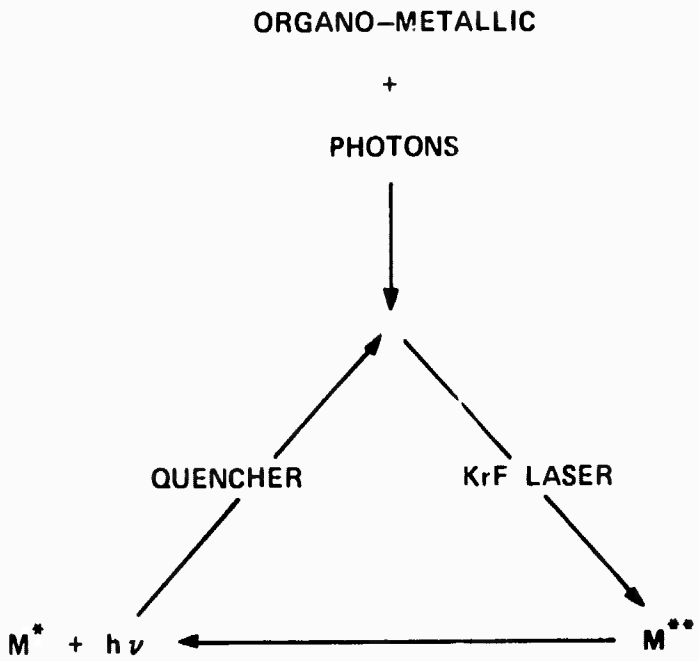

- KINETICS

LOSS	$M + M + X \rightarrow M_2 + X$	τ = 0.5 msec
RECYCLE	$M^* + Q \rightarrow M + Q$	τ = 3 nsec

H2771

Figure 23 Production and Recycling of Metal Atoms

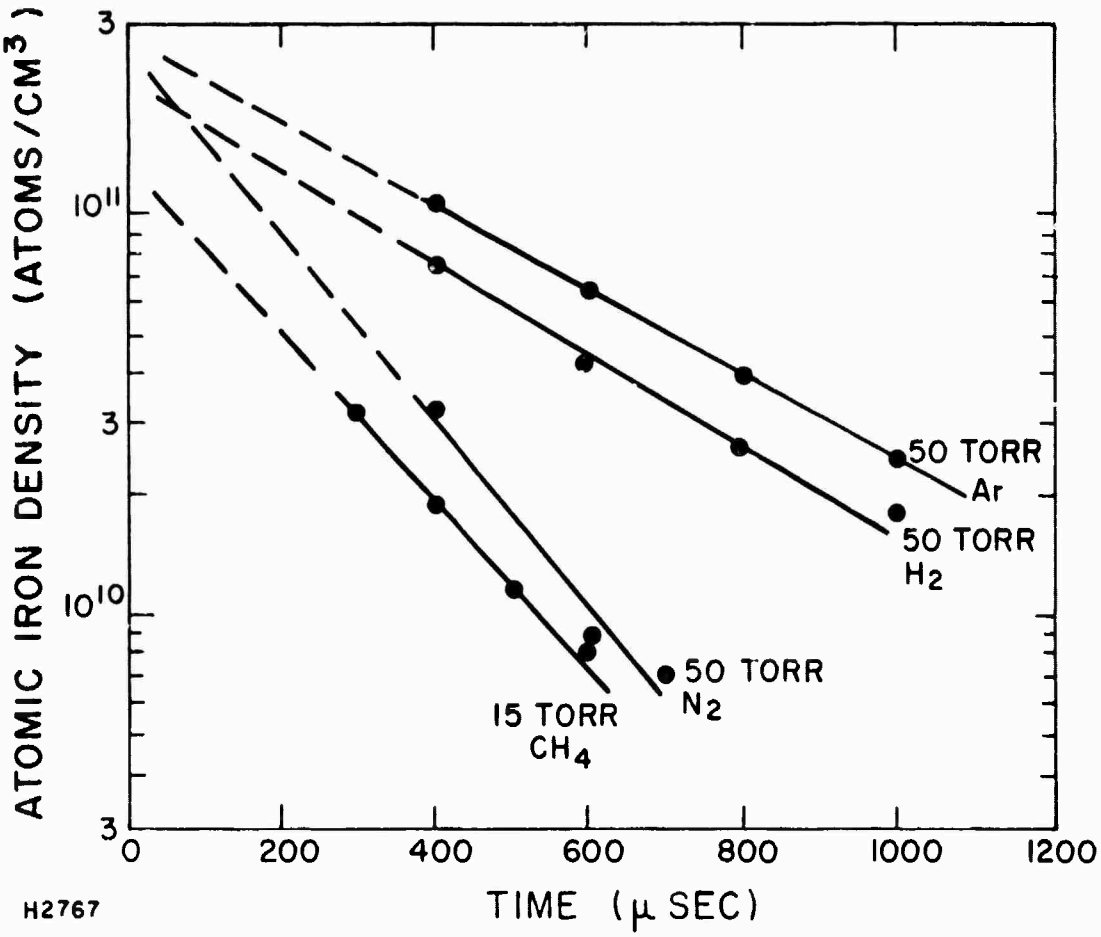

Figure 24 Quenching Gas Effects

presence of the surrounding gases, however, different quenchers exhibit efficiencies when acting as a third body, X, in the iron atom nucleation loss process (see Figure 23). Although these data are conveniently displayed as following exponential decay, the atoms are likely decaying according to the integrated solution for a third order process, i.e., $\frac{1}{[Fe]}$ vs time.

These experiments are continuing with our next efforts being directed toward calcium, whose production is limited to thermal techniques, but whose output is in a good wavelength region from propagation consideration.

2. Iron Pentacarbonyl, $Fe(CO)_5$

During the course of our investigation of the atomic iron laser discussed in the previous section, we observed stimulated emission from the organo-metallic precursor used in these experiments. A hint of this output can be seen in our initial experiments on atomic iron (see Figure 14) in the frame marked 'laser no discharge'. By optimizing the laser cell interaction volume and $Fe(CO)_5$ density, we were able to generate significant output at a number of wavelengths as shown in Figure 25. Using spectrally narrow filters, we were able to account for 60% of the output as being associated with the 384 nm transition. Most of the remaining photons are associated with the 562 nm line. The other observed transitions got stronger with repeated exposure of the same gas sample to a sequence of KrF laser pulses. It is likely they are due in some way to the $Fe_2(CO)_9$ formed by the action of UV light on $Fe(CO)_5$ by the following sequence.[17]

$$Fe(CO)_5 + h\nu \rightarrow\rightarrow Fe(CO)_4 + CO$$

(17) Eyber, G., Z. Physik Chem. 144A, 1 (1929).

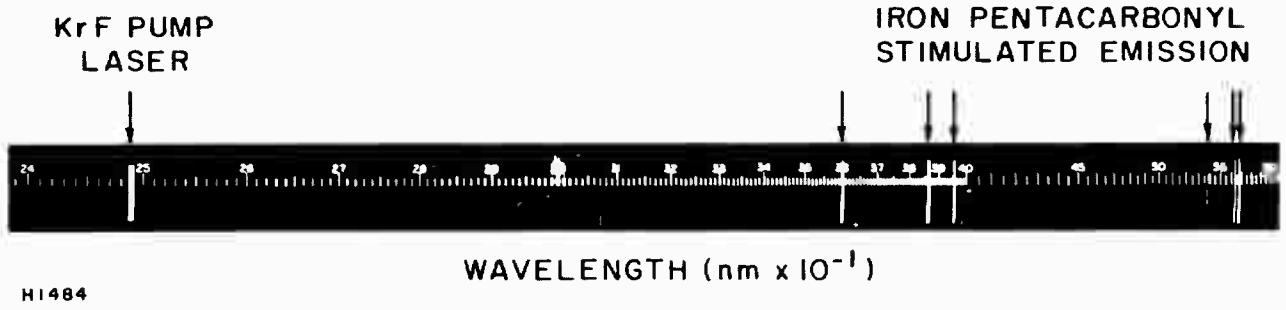

Figure 25 Optically Pumped Iron Pentacarbonyl Lasing Transitions

$$Fe(CO)_4 + Fe(CO)_5 \xrightarrow{(m)} Fe_2(CO)_9$$

We did however, see emission on those lines even on the first fill, but no special precautions were taken to isolate our storage containers from the action of the room lights, etc. and therefore there is likely to be $Fe_2(CO)_9$ "impurities" in the iron pentacarbonyl.

Since the output showed prompt temporal behavior (see Figure 26), it is likely to be lasing from an excited state of the $Fe(CO)_5$ or a photofragment produced in the initial photon absorption step, i.e.,

$$h\nu\ (KrF) + Fe(CO)_5 \rightarrow FeCO_5^{**}$$

$$Fe(CO)_5^{**} \rightarrow Fe(CO)_5^{*} + h\nu$$

$$Fe(CO)_5^{**} \rightarrow Fe(CO)_4^{**} + CO$$

$$Fe(CO)_4^{**} \rightarrow Fe(CO)_4^{*} + h\nu$$

We did see a trend with increased iron pentacarbonyl density (see Figure 27) and this behavior can be explained by recognizing that the extinction coefficient for $Fe(CO)_5$ absorption at 248 nm is 1.7×10^{-17} cm^2, (18) so for 0.2 torr, the distance for 50% extinction is 2.7 cm. We observed maximum output when the KrF pulse was focussed through a gas path length of approximately 4 cm. Increased converted output would be expected by reducing this to very short distances but severe damage to the optical window occurred for these cases. Clearly, pumping the iron carbonyl end-on (see Figure 20) in this matter is not optimal. We are, therefore, planning on using a cylindrical lens to transversely pump the $Fe(CO)_5$ in a dye cell configuration and look for output perpendicular to the pump laser.

(18) Lundquist, R. T. and Cris, M. J. Org. Chem 27, 1167 1962).

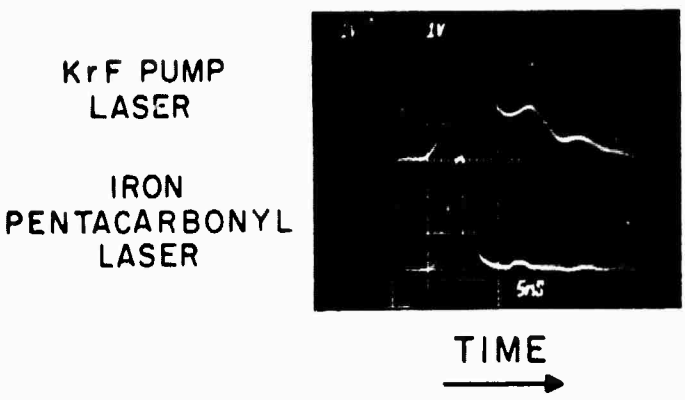

Figure 26 Experimental Data

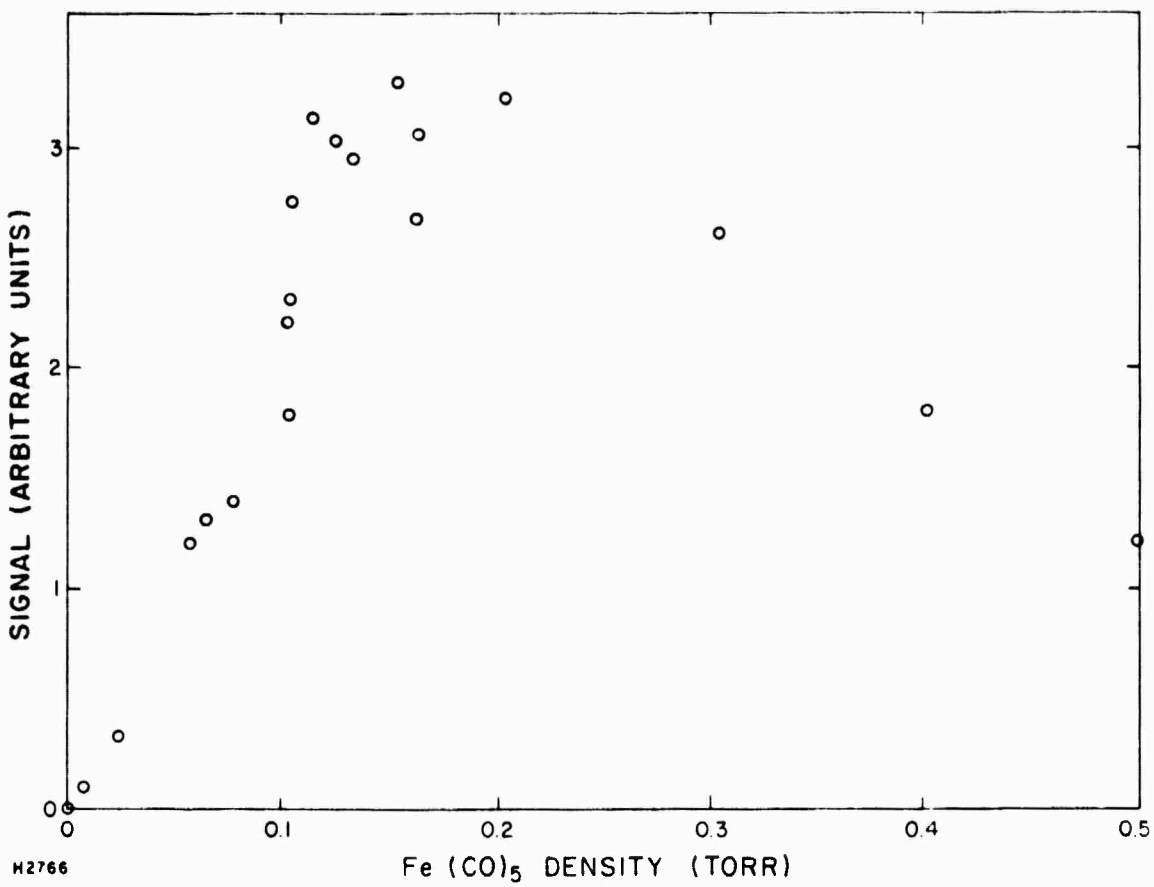

Figure 27 Variation of Output with $Fe(CO)_5$ Density

These experiments on photodissociation of encapsulated metals open a new field of candidates which do not require atom production techniques. If further research indicates efficient conversion can be achieved, the overall project would be simplified with regard to the engineering aspects of a practical device. More work in this area is continuing with emphasis being placed on transverse pumping, conversion efficiency, and new candidates.

IV. SUMMARY

With the delivery and modification of an untuned high power KrF laser, experiments began on optical conversion to longer wavelengths with various candidates generated using scalable production techniques. For ease of demonstration of principle, the candidates hydrogen, iron and calcium were identified as compatible with the available power and bandwidth of our pump laser and were therefore first considered. We lased hydrogen in the manner described in Reference 4 to calibrate our experimental setup and procedure. The next day we observed single pass amplified spontaneous emission from atomic iron produced by the discharge dissociation of $Fe(CO)_5$. In addition, we observed lasing in the organo-metallic precursor (i.e. the iron pentacarbonyl) where the inversion is from a molecular excited electronic state of the parent or a fragment produced in the photodissociation process. Experiments to evaluate this new class of conversion candidates and to demonstrate conversion in atomic calcium are continuing.

These results demonstrate that efficient conversion of KrF towards longer wavelengths is achievable using an untuned laser as the pump. Also, the technique of producing refractory metals in densities sufficiently high for single pass amplified spontaneous emission by the decomposition of organometallic compounds is clearly established.

In addition to the stimulated Raman candidates, the theoretical effort has identified a number of parametric acceptor candidates for converting KrF to more propagating wavelengths. An experimental evaluation of some of these candidates will be undertaken shortly.

THIS
PAGE
IS
MISSING
IN
ORIGINAL
DOCUMENT

REFERENCES

1. Parks, J.H., Appl. Phys. Letters 31, 192 (1977).

2. Parks, H.H., Appl. Phys. Letters 31, 297 (1977).

3. Djeu, N. and Burnham, R., Appl. Phys. Letters 30, 473 (1977).

4. Loree, T.R., Sze, R.C. and Barker, D.L., Appl. Phys. Letters 31, 37 (1977)

5. Trainor, D. W. and Mani, S.A., Optical Conversion Processes, Contract No. N00014-76-C-1162, Semi-Annual Technical Report, 15 Sept. 1976 to 15 March 1977.

6. Trainor, D.W. and Mani, S.A., 30th Annual Gaseous Electronics Conference, Paper #LA-3, 20 Oct. 1977.

7. Yuratich, M.A. and Hanna, D.C., J. Phys. B., Atom Molecular Phys. 9, 729 (1976)

8. Anderson, E.M., Anderson, E.R. and Trusov, V.F., Opt. Spectr. (USSR) 20, 471 (1966).

9. Gallagher, A. and Lurio, A., Phys. Rev. 136A, 87 (1964).

10. Vriens, L., Opt. Commun. 11, 396 (1974).

11. Miles, R.B. and Harris, E.E., I.E.E.E. - J.Q.E., QE-9, 470 (1973).

12. Nesmeyanov, An. N., Vapor Pressure of the Elements. (Academic Press, N.Y. 1963).

13. Moore, C.E., Atomic Energy Levels, Vol. III (N.B.S. circular 467, Washington, D.C., 1958).

14. Fano. V. and Cooper, J.W., Rev. Modern Phys. 40, 441 (1968).

15. Corliss, C.H. and Bozman , W. R., NBS Monograph 53 (1962).

16. Callear, A.B. and Oldman, R.I., Trans. Far. Soc. 63, 2888 (1967).

17. Eyber, G., Z. Physik Chem. 144A, 1 (1929).

18. Lundquist, R.T. and Cris, M.J., Org. Chem. 27, 1167 (1962).

DISTRIBUTION LIST

Office of Naval Research, Department of the Navy, Arlington, VA 22217 - Attn: Physics Program (3 copies)

Naval Research Laboratory, Department of the Navy, Washington, D.C. 20375 - Attn: Technical Library (1 copy)

Office of the Director of Defense, Research and Engineering, Information Office Library Branch, The Pentagon, Washington, D.C. 20301 (1 copy)

U.S. Army Research Office, Box CM, Duke Station, Durham, N.C. 27706 (1 copy)

Defense Documentation Center, Cameron Station, Alexandria, VA 22314 (12 copies)

Defender Information Analysis Center, Battelle Memorial Institute, 505 King Avenue, Columbus, OH 43201 (1 copy)

Commanding Officer, Office of Naval Research Branch Office, 536 South Clark Street, Chicago, IL 60615 (1 copy)

New York Area Office, Office of Naval Research, 715 Broadway (5th Floor), New York, NY 10003 - Attn: Dr. Irving Rowe (1 copy)

San Francisco Area Office, Office of Naval Research, 760 Market Street, Room 447, San Francisco, CA 94102 (1 copy)

Air Force Office of Scientific Research, Department of the Air Force, Washington, D.C. 22209 (1 copy)

Office of Naval Research Branch Office, 1030 East Green Street, Pasadena, CA 91106 - Attn: Dr. Robert Behringer (1 copy)

Code 102 IP (ONRL), Office of Naval Research, 800 N. Quincy Street, Arlington, VA 22217 (6 copies)

Defense Advanced Research Projects Agency, 1400 Wilson Blvd., Arlington, VA 22209 - Attn: Strategic Technology Office (1 copy)

Office Director of Defense, Research & Engineering, The Pentagon, Washington, D.C. 20301 - Attn: Assistant Director (Space and Advanced Systems) (1 copy)

Office of the Assistant Secretary of Defense, System Analysis (Strategic Programs), Washington, D.C. 20301 - Attn: Mr. Gerald R. McNichols (1 copy)

U.S. Arms Control and Disarmament Agency, Dept. of State Bldg., Rm. 4931, Washington, D.C. 2045) - Attn: Dr. Charles Henkin (1 copy)

Energy Research Development Agency, Division of Military Applications, Washington, D.C. 20545 (1 copy)

National Aeronautics and Space Administration, Lewis Research Center, Cleveland, OH 44135 - Attn: Dr. John W. Dunning, Jr. (1 copy)
(Aerospace Res. Engineer)

National Aeronautics & Space Administration, Code RR, FOB 10B, 600 Independence Ave., SW, Washington, D.C. 20546 (1 copy)

National Aeronautics and Space Administration, Ames Research Center, Moffett Field, CA 94035 - Attn: Dr. Kenneth W. Billman (1 copy)

Department of the Army, Office of the Chief of RD&A, Washington, D.C. 20310 - Attn: DARD-DD (1 copy)
DAMA-WSM-T (1 copy)

Department of the Army, Office of the Deputy Chief of Staff for Operations & Plans, Washington, D.C. 20310 - Attn: DAMO-RQD - (1 copy)

Ballistic Missile Defense Program Office (BMDPO), The Commonwealth Building, 1300 Wilson Blvd., Arlington, VA 22209 - Attn: Mr. Albert J. Bast, Jr. (1 copy)

U.S. Army Missile Command, Research & Development Division, Redstone Arsenal, AL 35809 - Attn: Army High Energy Laser Programs (2 copies)

Commander, Rock Island Arsenal, Rock Island, IL 61201, Attn: SARRI-LR, Mr. J.W. McGarvey (1 copy)

Commanding Officer, U.S. Army Mobility Equipment R&D Center, Ft. Belvoir, VA 22060 - Attn: SMEFB-MW (1 copy)

Commander, U.S. Army Armament Command, Rock Island, IL 61201 - Attn: AMSAR-RDT (1 copy)

Director, Ballistic Missile Defense Advanced Technology Center, P.O. Box 1500, Huntsville AL 35807 - Attn: ATC-O (1 copy)
ACT-T (1 copy)

Commander, U.S. Army Material Command, Alexandria, VA 22304 - Attn: Mr. Paul Chernoff (AMCRD-T) (1 copy)

Commanding General, U.S. Army Munitions Command, Dover, NH 17801 - Attn: Mr. Gilbert F. Chesnov (AMSMU-R) (1 copy)

Director, U.S. Army Ballistics Res. Lab, Aberdeen Proving Ground, MD 21005 - Attn: Dr. Robert Eichenberger (1 copy)

Commandant, U.S. Army, Air Defense School, Ft. Bliss, TX 79916 - Attn: Air Defense Agency (1 copy)
ATSA-CTD-MS (1 copy)

Commanding General, U.S. Army Combat Dev. Command, Ft. Belvoir, VA 22060 - Attn: Director of Material, Missile Div. (1 copy)

Commander, U.S. Army Training & Doctrine Command, Ft. Monroe, VA. 23651 - Attn: ATCD-CF (1 copy)

Commander, U.S. Army Frankford Arsenal, Philadelphia, PA 19137 - Attn: Mr. M. Elnick SARFA-FCD Bldg. 201-3 (1 copy)

Commander, U.S. Army Electronics Command, Ft. Monmouth, NJ 07703 - Attn: AMSEL-CT-L, Dr. R.G. Buser (1 copy)

Commander, U.S. Army Combined Arms Combat Developments Activity, Ft. Leavenworth, KS 66027 (1 copy)

National Security Agency, Ft. Geo. G. Meade, MD 20755 - Attn: R.C. Foss A763 (1 copy)

Deputy Commandant for Combat & Training Developments, U.S. Army Ordnance Center and School, Aberdeen Proving Ground, MD 21005
Attn: ATSL-CTD-MS-R (1 copy)

Commanding Officer, USACDC CBR Agency, Ft. McClellan, AL 36201 - Attn: CDCCBR-MP (Mr. F.D. Poer) (1 copy)

DISTRIBUTION LIST (Continued)

Department of the Navy, Office of the Chief of Naval Operations, The Pentagon 5C732 - Washington, D.C. 20350 - Attn: (OP-982J1) (1 copy)

Office of Naval Research Branch Office, 495 Summer Street, Boston, MA 02210 - Attn: Dr. Fred Quelle (1 copy)

Department of the Navy, Deputy Chief of Navy Material (Dev.), Washington, D.C. 20360 - Attn: Mr. R. Gaylord (MAT 032B) (1 copy)

Naval Missile Center, Point Mugu, CA 93042 - Attn: Gary Gibbs (Code 5352) (1 copy)

Naval Research Laboratory, Washington, D.C. 20375 - Attn: (Code 5503-EOTPO) (1 copy)
Dr. P. Livingston - Code 5560 (1 copy)
Dr. A. L. Schindler - Code 6000 (1 copy)
Dr. H. Shenker - Code 5504 (1 copy)
Mr. D. J. McLaughlin - Code 5560 (1 copy)
Dr. John L. Walsh - Code 5503 (1 copy)

High Energy Laser Project Office, Department of the Navy, Naval Sea Systems Command, Washington, D.C. 20360 - Attn: Capt. A. Skolnick, USN (PMS 22) (1 copy)

Superintendent, Naval Postgraduate School, Monterey, CA 93940 - Attn: Library (Code 2124) (1 copy)

Navy Radiation Technology, Air Force Weapons Lab (NLO), Kirtland AFB, NM 87117 (1 copy)

Naval Surface Weapons Center, White Oak, Silver Spring, MD 20910 - Attn: Dr. Leon H. Schindel (Code 310) (1 copy)
Dr. E. Leroy Harris (Code 313) (1 copy)
Mr. K. Enkenhaus (Code 044) (1 copy)
Mr. J. Wise (Code 047) (1 copy)
Technical Library (1 copy)

U.S. Naval Weapons Center, China Lake, CA 93555 - Attn: Technical Library (1 copy)

HQ USAF (AF/RDPS), The Pentagon, Washington, D.C. 20330 - Attn: Lt. Col. A.J. Chiota (1 copy)

HQ AFSC/XRLW, Andrews AFB, Washington, D.C. 20331 - Attn: Maj. J.M. Walton (1 copy)

HQ AFSC (DLCAW), Andrews AFB, Washington, D.C. 20331 - Attn: Maj. H. Axelrod (1 copy)

Air Force Weapons Laboratory, Kirtland AFB, NM 87117 - Attn: LR (1 copy)
AL (1 copy)

HQ SAMSO (XRTD), P.O. Box 92960, Worldway Postal Center, Los Angeles, CA 90009 - Attn: Lt. Dorian DeMaio (XRTD) (1 copy)

AF Avionics Lab (TEO), Wright Patterson AFB, OH 45433 - Attn: Mr. K. Hutchinson (1 copy)

Dept. of the Air Force, Air Force Materials Lab. (AFSC), Wright Patterson AFB, OH 45433 - Attn: Maj. Paul Elder (LPS) (1 copy)
Laser Window Group

HQ Aeronautical Systems Div., Wright Patterson AFB, OH 45433 - Attn: XRF - Mr. Clifford Fawcett (1 copy)

Rome Air Development Command, Griffiss AFB, Rome, NY 13440 - Attn: Mr. R. Urtz (OCSE) (1 copy)

HQ Electronics Systems Div. (ESL), L.G. Hanscom Field, Bedford, MA 01730 - Attn: Mr. Alfred E. Anderson (XRT) (1 copy)
Technical Library (1 copy)

Air Force Rocket Propulsion Lab., Edwards AFB, CA 93523 - Attn: B.R. Bornhorst, (LKCG) (1 copy)

Air Force Aero Propulsion Lab., Wright Patterson AFB, OH 45433 - Attn: Col. Walter Moe (CC) (1 copy)

Dept. of the Air Force, Foreign Technology Division, Wright Patterson AFB, OH 45433 - Attn: PDIN (1 copy)

Commandant of the Marine Corps, Scientific Advisor (Code RD-1), Washington, D.C. 20380 (1 copy)

Aerospace Research Labs., (AP), Wright Patterson AFB, OH 45433 - Attn: Lt. Col. Max Duggins (1 copy)

Defense Intelligence Agency, Washington, D.C. 20301 - Attn: Mr. Seymour Berler (DIAB) (1 copy)

Central Intelligence Agency, Washington, D.C. 20505 - Attn: Mr. Julian C. Nall (1 copy)

Analytic Services, Inc., 5613 Leesburg Pike, Falls Church, VA 22041 - Attn: Dr. John Davis (1 copy)

Aerospace Corp., P.O. Box 92957, Los Angeles, CA 90009 - Attn: Dr. G.P. Millburn (1 copy)

Airesearch Manuf. Co., 9851-9951 Sepulveda Blvd., Los Angeles, CA 90009 - Attn: Mr. A. Colin Stanclife (1 copy)

Atlantic Research Corp., Shirley Highway at Edsall Road, Alexandria, VA 22314 - Attn: Mr. Robert Naismith (1 copy)

Avco Everett Research Lab., 2385 Revere Beach Parkway, Everett, MA 02149 - Attn: Dr. George Sutton (1 copy)
Dr. Jack Daugherty (1 copy)

Battelle Columbus Laboratories, 505 King Avenue, Columbus, OH 43201 - Attn: Mr. Fred Tietzel (STPIAC) (1 copy)

Bell Aerospace Co., Buffalo, NY 14240 - Attn: Dr. Wayne C. Solomon (1 copy)

Boeing Company, P.O. Box 3999, Seattle, WA 98124 - Attn: Mr. M.I. Gamble (2-, 450, MS 8C-88) (1 copy)

Electro Optical Systems, 300 N. Halstead, Pasadena, CA 91107 - Attn: Dr. Andrew Jensen (1 copy)

ESL, Inc., 495 Java Drive, Sunnyvale, CA 94086 - Attn: Arthur Einhorn (1 copy)

DISTRIBUTION LIST (Continued)

General Electric Co., Space Division, P.O. Box 8555, Philadelphia, PA 19101 - Attn: Dr. R.R. Siglemonti (1 copy)

General Electric Co., 100 Plastics Avenue, Pittsfield, MA 01201 - Attn: Mr. D.G. Harrington (Rm. 1044) (1 copy)

General Research Corp., P.O. Box 3587, Santa Barbara, CA 93105 - Attn: Dr. R. Holbrook (1 copy)

General Research Corp., 1501 Wilson Blvd., Suite 700, Arlington, VA 22209 - Attn: Dr. Giles F. Crimi (1 copy)

Hercules, Inc., Industrial System Dept., Wilmington, DE 19899 - Attn: Dr. R.S. Voris (1 copy)

Hercules, Inc., P.O. Box 210, Cumberland, MD 21502 - Attn: Dr. Ralph R. Preckel (1 copy)

Hughes Research Labs., 3011 Malibu Canyon Road, Malibu, CA 90265 - Attn: Dr. D. Forster (1 copy)

Hughes Aircraft Co., Aerospace Group - Systems Division, Canoga Park, CA 91304 - Attn: Dr. Jack A. Alcalay (1 copy)

Hughes Aircraft Co., Centinela and Teale Streets, Bldg. 6, MS E-125, Culver City, CA 90230 - Attn: Dr. William Yates (1 copy)

Institute for Defense Analyses, 400 Army-Navy Drive, Arlington, VA 22202 - Attn: Dr. Alvin Schnitzler (1 copy)

Johns Hopkins University, Applied Physics Lab., 8621 Georgia Avenue, Silver Spring, MD 20910 - Attn: Dr. Albert M. Stone (1 copy)

Lawrence Livermore Laboratory, P.O. Box 808, Livermore, CA 94550 - Attn: Dr. R.E. Kidder (1 copy)
Dr. E. Teller (1 copy)
Dr. Joe Fleck (1 copy)

Los Alamos Scientific Laboratory, P.O. Box 1663, Los Alamos, NM 87544 - Attn: Dr. Keith Boyer (1 copy)

Lulejian and Associates, Inc., Del Amo Financial Center, 21515 Hawthorne Blvd. - Suite 500, Torrance, CA 90503 (1 copy)

Lockheed Palo Alto Res. Lab., 3251 Hanover St., Palo Alto, CA 94303 - Attn: L.R. Lunsford, Orgn. 52-24, Bldg. 201 (1 copy)

Mathematical Sciences Northwest, Inc., P.O. Box 1887, Bellevue, WN 98009 - Attn: Dr. Abraham Hertzberg (1 copy)

Martin Marietta Corp., P.O. Box 179, Mail Station 0471, Denver, CO 80201 - Attn: Mr. Stewart Chapin (1 copy)

Massachusetts Institute of Technology, Lincoln Laboratory, P.O. Box 73, Lexington, MA 02173 - Attn: Dr. S. Edelberg (1 copy)
Dr. L.C. Marquet (1 copy)

McDonnell Douglas Astronautics Co., 5301 Bolsa Avenue, Huntington Beach, CA 92647 - Attn: Mr. P.L. Klevatt, Dept. A3-830-BBFO, M/S 9 (1 copy)

McDonnell Douglas Research Labs., Dept. 220, Box 516, St. Louis, MO 63166 - Attn: Dr. D.P. Ames (1 copy)

MITRE Corp., P.O. Box 208, Bedford, MA 01730 - Attn: Mr. A.C. Cron (1 copy)

North American Rockwell Corp., Autonetics Div., Anaheim, CA 92803 - Attn: Mr. T.T. Kumagi, C/ Mail Code HA18 (1 copy)

Northrop Corp., 3401 West Broadway, Hawthorne, CA 90250 - Attn: Dr. Gerard Hasserjian, Laser Systems Dept. (1 copy)

Dr. Anthony N. Pirri, Physical Sciences, Inc., 18 Lakeside Office Park, Wakefield, MA 01880 (1 copy)

RAND Corp., 1700 Main Street, Santa Monica, CA 90406 - Attn: Dr. C.R. Culp/Mr. G.A. Carter (1 copy)

Raytheon Co., 28 Seyon Street, Waltham, MA 02154 - Attn: Dr. F.A. Horrigan (Res. Div.) (1 copy)

Raytheon Co., Boston Post Road, Sudbury, MA 01776 - Attn: Dr. C. Sonnenschien (Equip. Div.) (1 copy)

Raytheon Co., Bedford Labs, Missile Systems Div., Bedford, MA 01730 - Attn: Dr. H.A. Mehlhorn (1 copy)

Riverside Research Institute, 80 West End Street, New York, NY 10023 - Attn: Dr. L.H. O'Neill (1 copy)
Dr. John Bose (1 copy)
(HPEGL Library) (1 copy)

R&D Associates, Inc., P.O. Box 3580, Santa Monica, CA 90431 - Attn: Dr. R.E. LeLevier (1 copy)

Rockwell International Corporation, Rocketdyne Division, Albuquerque District Office, 3636 Menaul Blvd., NE, Suite 211, Albuquerque, NM 87110 - Attn: C.K. Kraus, Mgr. (1 copy)

SANDIA Corp., P.O. Box 5800, Albuquerque, NM 87115 - Attn: Dr. Al Narath (1 copy)

Stanford Research Institute, Menlo Park, CA 94025 - Attn: Dr. F.T. Smith (1 copy)

Science Applications, Inc., 1911 N. Ft. Meyer Drive, Arlington, VA 22209 - Attn: L. Peckam (1 copy)

Science Applications, Inc., P.O. Box 328, Ann Arbor, MI 48103 - Attn: R.E. Meredith (1 copy)

Science Applications, Inc., 6 Preston Court, Bedford, MA 01703 - Attn: R. Greenberg (1 copy)

Science Applications, Inc., P.O. Box 2351, La Jolla, CA 92037 - Attn: Dr. John Asmus (1 copy)

Systems, Science and Software, P.O. Box 1620, La Jolla, CA 92037 - Attn: Alan F. Klein (1 copy)

Systems Consultants, Inc., 1050 31st Street, NW, Washington, D.C. 20007 - Attn: Dr. R.B. Keller (1 copy)

Thiokol Chemical Corp., WASATCH Division, P.O. Box 524, Brigham City, UT 84302 - Attn: Mr. J.E. Hansen (1 copy)

TRW Systems Group, One Space Park, Bldg. R-1, Rm. 1050, Redondo Beach, CA 90278 - Attn: Mr. Norman Campbell (1 copy)

United Technologies Research Center, 400 Main Street, East Hartford, CT 06108 - Attn: Mr. G.H. McLafferty (3 copies)

DISTRIBUTION LIST (Continued)

United Technologies Research Center, Pratt and Whitney Aircraft Div., Florida R&D Center, West Palm Beach, FL 33402 Attn: Dr. R.A. Schmidtke (1 copy)
Mr. Ed Pinsley (1 copy)

VARIAN Associates, EIMAC Division, 301 Industrial Way, San Carlos, CA 94070 - Attn: Mr. Jack Quinn (1 copy)

Vought Systems Division, LTV Aerospace Corp., P.O. Box 5907, Dallas, TX 75222 - Attn: Mr. F G. Simpson, MS 254142 (1 copy)

Westinghouse Electric Corp., Defense and Space Center, Balt-Wash. International Airport - Box 746, Baltimore, MD 21203 - Attn: Mr. W.F. List (1 copy)

Westinghouse Research Labs., Beulah Road, Churchill Boro, Pittsburgh, PA 15235 - Attn: Dr. E.P. Riedel (1 copy)

United Technologies Research Center, East Hartford, CT 06108 - Attn: A.J. DeMaria (1 copy)

Airborne Instruments Laboratory, Walt Whitorlan Road, Melville, NY 11746 Attn: F. Pace (1 copy)

General Electric R&D Center, Schenectady, NY 12305 - Attn: Dr. Donald White (1 copy)

Cleveland State University, Cleveland, OH 44115 - Attn: Dean Jack Scales (1 copy)

EXXON Research and Engineering Co., P.O. Box 8, Linden, NJ 07036 - Attn: D. Grafstein (1 copy)

University of Maryland, Department of Physics and Astronomy, College Park, MD 20742 - Attn: D. Currie (1 copy)

Sylvania Electric Products, Inc., 100 Fergeson Drive, Mountain View, CA 94040 - Attn: L.M. Osterink (1 copy)

North American Rockwell Corp., Autonetics Division, 3370 Miraloma Avenue, Anaheim, CA 92803 - Attn: R. Gudmundsen (1 copy)

Massachusetts Institute of Technology, 77 Massachusetts Avenue, Cambridge, MA 02138 - Attn: Prof. A. Javan (1 copy)

Lockheed Missile & Space Co., Palo Alto Research Laboratories, Palo Alto, CA 94304 - Attn: Dr. R.C. Ohlman (1 copy)

ILC Laboratories, Inc., 164 Commercial Street, Sunnyvale, CA 94086 - Attn: L. Noble (1 copy)

University of Texas at Dallas, P.O. Box 30365, Dallas, TX 75230 - Attn: Prof. Carl B. Collins (1 copy)

Polytechnic Institute of New York, Rt. 110, Farmingdale, NY 11735 - Attn: Dr. William T Walter (1 copy)